https://doi.org/10.5194/acp-2022-458
Preprint. Discussion started: 4 July 2022

Atmospheric Chemistry and Physics Discussions

Monitoring and assimilation of S5P/TROPOMI carbon monoxide data with the global CAMS near-real time system

Antje Inness[1], Ilse Aben[2], Melanie Ades[1], Tobias Borsdorff[2], Johannes Flemming[1], Jochen Landgraf[2], Bavo Langerock[3], Mark Parrington[1] and Roberto Ribas[1]

[1]ECMWF, Shinfield Park, Reading, RG2 9AU, UK
[2]SRON Netherlands Institute for Space Research, Leiden, the Netherlands
[3]BIRA-IASB, 1180 Brussels, Belgium

Correspondence to: Antje Inness (a.inness@ecmwf.int)

Abstract. The Tropospheric Monitoring Instrument (TROPOMI) on the Copernicus Sentinel 5 Precursor (S5P) satellite, launched in October 2017, provides a wealth of atmospheric composition data, including total columns of carbon monoxide (TCCO) at high horizontal resolution (5.5 km x 7 km). Near-real time TROPOMI TCCO data have been monitored in the global data assimilation system of the Copernicus Atmospheric Monitoring Service (CAMS) since November 2018 to assess the quality of the data. The CAMS system already routinely assimilates TCCO data from the Measurement of Pollution in the Troposphere (MOPITT) instrument and the Atmospheric Sounding Interferometer (IASI) outside the polar regions. In the global mean, CAMS TCCO analysis values are about 10% lower than TROPOMI TCCO when only IASI and MOPITT thermal infrared (TIR) TCCO data are assimilated (averaged over the period November 2018 to Dec 2021), with the largest relative differences (11-14%) found in the polar latitude bands, i.e., the areas where no satellite CO retrievals are assimilated in the global CAMS system. Most of these differences are due to a low TCCO bias of the CAMS model, rather than a high bias of TROPOMI.

The assimilation of NRT TROPOMI TCCO data in the CAMS system was tested for the period 2021-07-06 to 2021-12-31, i.e., after the TROPOMI algorithm update to version 02.02.00 in July 2021. It leads to a much-improved CO analysis field, with increased CO values and improved fit to independent observations, such as IAGOS aircraft profiles, NDACC FTIR tropospheric and total column CO data, as well as surface CO data from the Air Now, AirBase and Chinese air quality networks. The largest absolute and relative changes from the assimilation of TROPOMI CO, in addition to the already assimilated IASI and MOPITT TIR TCCO data, are found in the lower and mid troposphere, i.e., that part of the atmosphere that is not already well constrained by the already assimilated TIR MOPITT and IASI data. The largest impact near the surface comes from clear-sky TROPOMI data over land, and additional vertical information comes from the retrievals of measurements in cloudy conditions.

July and August 2021 saw record numbers of boreal wildfires over North America and Russia leading to large amounts of CO being released into the atmosphere. The CAMS CO analysis captures the high CO columns resulting from these fires and also shows plumes of high CO from the boreal wildfires that are transported from Siberia over the North Pole and from North America over the North Atlantic reaching as far as Europe, even though some of the high CO values detected in the upper troposphere by IAGOS aircraft that intersected parts of the plumes are not quite reached in the CAMS CO analysis.

1 Introduction

The Copernicus Atmosphere Monitoring Service (CAMS, atmosphere.copernicus.eu), implemented by the European Centre for Medium Range Weather Forecasts (ECMWF) as part of the European Union's Copernicus Programme, produces daily

https://doi.org/10.5194/acp-2022-458
Preprint. Discussion started: 4 July 2022

Atmospheric Chemistry and Physics Discussions

global near-real time (NRT) forecasts of atmospheric composition up to five days ahead. To improve the quality of the CAMS forecasts the initial conditions for some of the chemical species, including Carbon Monoxide (CO), Nitrogen Dioxide (NO_2), Ozone (O_3), Sulphur Dioxide (SO_2) and for aerosols are provided by assimilating satellite retrievals of atmospheric composition using ECMWF's 4-dimensional variations (4D-Var) data assimilation system (Remy et al., 2019; Inness et al., 2019a, 2019b, 2015a; Benedetti et al., 2009). The CAMS global NRT system is constantly advanced and improved through updates to the chemical scheme, the NWP model, and by including additional satellite retrievals from new satellite instruments as they become available, as documented in Inness et al. (2019b).

A wealth of new atmospheric composition data became available with the launch of the Sentinel 5-Precursor (S5P) satellite in October 2017. S5P carries the TROPOspheric Monitoring Instrument (TROPOMI) which provides high-resolution spectral measurements in the ultraviolet (UV), visible (VIS), near infrared (NIR) and shortwave-infrared (SWIR) part of the spectrum. This wide spectral range allows the retrieval of several atmospheric pollutants species, including O_3, NO_2, SO_2 and Formaldehyde (HCHO) from the UVVIS, and CO and Methane (CH_4) from the SWIR part of the spectrum (Veefkind et al, 2012). These species are all forecast by the CAMS global system, making TROPOMI the perfect instrument to provide observations for the CAMS NRT analysis at unprecedented horizontal resolution of about 5.5 km x 3.5 km for the species retrieved in the UV/VIS and 5.5 km x 7 km for CO and CH_4 retrieved from the SWIR. TROPOMI S5P has been operational since April 2018, and TROPOMI NRT CO data have been routinely monitored in the CAMS global NRT system since November 2018.

Carbon monoxide has natural and anthropogenic sources (Seinfeld and Pandis, 2006; Kanakidou and Crutzen, 1999). Its main sources are incomplete fossil fuel and biomass burning (Worden et al., 2013), which lead to enhanced surface concentrations, and in-situ production via the oxidation of CH_4, isoprene and other organic trace gases. Combustion and chemical in-situ sources can produce similar amounts of CO on the global scale (Gaubert et al., 2016) but vary in space and time because of the changing distribution of anthropogenic and wildfire CO emissions as well as of the biogenic isoprene emissions. In seasonal means, the largest CO concentrations are found over the industrial regions of Asia, North America and Europe, and over the tropical biomass burning areas. However, in areas with large biogenic emissions (e.g., tropical forests), oxidation of biogenic volatile organic compounds (VOCs) contributes strongly to the production of CO (Griffin et al. 2007). Hudman et al. (2008) found that over the Eastern US during summer the biogenic sources of CO were higher than the anthropogenic ones. Boreal and Austral wildfires can also lead to increased CO abundances outside the tropics. Tropical and extratropical wildfires show large inter annual variability leading to pronounced CO anomalies in certain years (Flemming and Inness, 2021; Inness et al., 2015b). The main loss process for CO is the reaction with the hydroxyl radical (OH). CO surface concentrations are higher during local winter than during the summer months because of the shorter CO lifetime in summer due to higher OH concentrations and more intense mixing processes. Tropical biomass burning is most intense during the dry season (December-April in the Northern Hemisphere (NH) tropics, July-October in the Southern Hemisphere (SH) tropics). CO has a lifetime of several weeks and can serve as a tracer for regional and inter-continental transport of polluted air. CO is an indirect short-lived climate forcer because it is an important precursor for tropospheric ozone (Szopa et al., 2021, section 6.3.3.2), and because it impacts OH, which controls the lifetime of CH_4.

Before new data can be assimilated in the CAMS NRT analysis, the quality of the data in relation to the current system must be established. This is usually done by including the data passively in the data assimilation system, so that statistics of the differences between the observations and collocated model fields can be calculated without the data influencing the analysis and subsequent forecast (Inness et al., 2019b, Garrigues et al., 2022). We call this 'monitoring' of the observations. The model fields are interpolated in time and space to the location of the observations, and the model equivalents of the observations are

https://doi.org/10.5194/acp-2022-458
Preprint. Discussion started: 4 July 2022


Atmospheric Chemistry and Physics Discussions

calculated, e.g., by applying the averaging kernels of the observations to the model fields. Temporal and spatial statistics of the differences between the model fields and the observations can then be analysed.

The differences between the observations and the model equivalents are called departures. We distinguish between first-guess departures (observations minus model first-guess field) and analysis departures (observations minus analysed field). The first-guess field is the model forecast from the previous analysis, i.e., before the fields are changed by the analysis increments. Long-term monitoring of the departures can disclose errors and biases in the satellite data products, as well as errors or biases in the model. Because the departures are usually small, they show up changes more clearly than when looking at the absolute model fields or observation values. A sudden jump on a global scale, which is larger than the instrument noise, can be an indication of problems in the observations or the model. The advantage of using an assimilation system to monitor satellite data is that it provides continuous global coverage and allows us to build up global and regional statistics quickly. If the monitoring results show the data to be of good quality, i.e., departures are stable, there are no sudden jumps, the biases with respect to the model are not too large, assimilation tests with the data begin, followed by the operational use of the data in the CAMS global NRT system.

Initial work about the use of early TROPOMI CO data in the CAMS system was published in an ECMWF technical memorandum (Inness et al., 2019c) but not in a peer reviewed publication. The current work makes use of a much longer timeseries and more mature retrieval version of TROPOMI CO data, contains a lot of additional work, and documents the preparation of the global CAMS NRT system for the routine NRT assimilation of TROPOMI total columns CO (TCCO) data. For this, we assess the NRT TROPOMI TCCO product and compare it with the global CAMS NRT CO analysis for the period from 19 November 2018 to 31 December 2021, and we present results from assimilation tests with the NRT TROPOMI TCCO data for the period 6 July to 31 December 2021. The paper is structured in the following way. Section 2 describes the CAMS model and data assimilation system as well as the NRT TROPOMI TCCO data product and how the data are included in the global CAMS system. Section 3 shows results from the monitoring of TROPOMI TCCO data with the NRT CAMS system, and Section 4 shows results from assimilation tests with the TROPOMI TCCO data, validating the resulting CO analyses with independent observations. Section 5 gives the conclusions.

2 Model and Observations

2.1 CAMS system and CO analysis

2.1.1 CAMS model and data assimilation system

The CAMS model and data assimilation system is a specific configuration based on ECMWF's integrated Forecast System (IFS). The chemical mechanism of the IFS versions used between 2018 and 2021 is an extended version of the Carbon Bond Mechanism 5 (CB05, Huijnen et al. 2010) as implemented in Chemical Transport Model (CTM) Transport Model 5 (TM5). It is documented in Flemming et al. (2015, 2017) and more recent updates in Inness et al. (2019a) and Huijnen et al. (2019). CB05 is a tropospheric chemistry scheme with 57 species and 131 reactions. The horizontal resolution of the CAMS model is approximately 40 km (T511 linear spectral truncation and 0.35° by 0.35° grid), i.e., coarser than the resolution of the TROPOMI data.

The NRT global CAMS system has used CAMS-GLOBANT anthropogenic emissions (Granier et al., 2019) since July 2019 and used MACCity anthropogenic emissions (Granier et al., 2011) before then. Biomass burning emissions have come from the Global Fire Assimilation System V1.4 (GFAS, Kaiser et al., 2012) since October 2020 and were GFAS V1.2 before.

https://doi.org/10.5194/acp-2022-458
Preprint. Discussion started: 4 July 2022

Atmospheric Chemistry and Physics Discussions

Biogenic emissions are from CAMS-GLOBBIO since July 2019, based on the Model of Emissions of Gases and Aerosols from Nature (MEGAN, Guenther et al., 2006), and from MEGAN_MACC, a different application of the MEGAN model, before then (see also Table 2 below for CAMS model changes).

The IFS uses an incremental four-dimensional variational (4D-Var) data assimilation system going back to Courtier et al. (1994). In the current CAMS 4D-Var setup, a cost function that measures the differences between the model fields and the observations is minimized to obtain the best possible forecast through the length of the assimilation window by adjusting the initial conditions. Several atmospheric composition fields, including CO, are included in the control vector and minimized together with the meteorological control variables. The data assimilation methodology for the atmospheric composition fields remains unchanged to the one described in Inness et al. (2015a) but the background errors for CO were updated in July 2019 (Figure 1). CAMS uses 12-hour assimilation windows from 03 UTC to 15 UTC and 15 UTC to 3 UTC, and two minimisations at spectral truncations T95 (~ 210 km) and T159 (~ 110 km).

TCCO products from IASI and MOPITT instruments are routinely assimilated in the CAMS NRT system (see Table 1). The MOPITT data used by CAMS are the thermal infrared (TIR) MOPITT retrievals from the 4.7 µm band (Deeter et al., 2017, 2019, 2021). IASI TCCO is retrieved from the same band (spectral range 2143-2181.25 cm^{-1}), and the data used during the period covered in this paper are produced by Eumetsat using LATMOS/ULB's Fast Optimal Retrievals on Layers for IASI (FORLI, v20151001) algorithm, documented in George et al. (2009) and Clerbaux et al. (2009). The TIR retrievals have the largest sensitivity to CO in the mid troposphere (Deeter et al., 2013; George et al., 2015). In the CAMS system IASI and MOPITT TCCO data are thinned to a horizontal resolution of 0.5° x 0.5° by randomly selecting one observation in each grid cell.

Table 1: Satellite TCCO data products used or monitored in the global CAMS NRT system since November 2018. VarBC stands for variational bias correction, LAT denotes latitude, SOE solar elevation, QF the overall quality flags given by the data providers (QF=0 for good data) and qa_value a quality assurance flag given in the TROPOMI data.

Instrument/ Satellite	Data provider/ version	Blacklist criteria / thinning	VarBC Predictors for CO	Reference
IASI/ Metop-A (until 20191031) Metop-B Metop-C (since 20191101)	Eumetsat, NRT	QF>0 Abs(LAT)<65º SOE<5º Thinned to 0.5ºx0.5º	Global constant, 1000-300 hPa thickness, thermal contrast (over land)	George et al. (2009), Clerbaux et al. (2009)
MOPITT/Terra (TIR)	NASA, V7 NRT (until 20190630) V8 NRT (until 20211009) V9 NRT (since 20211010)	QF>0 Abs(LAT)<65º Night-time data over Greenland Thinned to 0.5ºx0.5º	Not applied	Deeter et al. (2017) Deeter et al. (2019) Deeter et al. (2021)
TROPOMI/ Sentinel-5P	ESA/ SRON NRT (see Table 3)	qa_value<0.5 LAT<60ºS Clear data over ocean Super-obbed to T511 (see section 2.3)	Not applied	Landgraf et al. (2016)

The observation operator for TCCO in the CAMS system applies the averaging kernels of the observations to the model fields and calculates the model equivalent at the observation location and time, giving departures between the observations and the model as:

$$d = y - \hat{H}(x_m) \quad (1)$$

Here, d is the departure between observation and model equivalent in observation space, y the TCCO retrieval, $\hat{H}$ the observation operator to calculate the model equivalent of the observations from the 137 model level fields (x_m). Neglecting

https://doi.org/10.5194/acp-2022-458
Preprint. Discussion started: 4 July 2022

Atmospheric Chemistry and Physics Discussions

any error terms, the TCCO retrievals can be written using the averaging kernel A, that relates the true vertical CO profile x_t to the retrieved total columns

$$y = x_{ap} + A(x_t - x_{ap}) \quad (2)$$

where x_{ap} is an apriori profile used in the retrieval of y. In the observation operator we apply the averaging kernels A to the model profiles, x_m, to smooth the model profiles according to the sensitivity of the retrievals. This means Equation (1) can be written as

$$d = x_{ap} + A(x_t - x_{ap}) - \left(x_{ap} + A(H(x_m) - x_{ap})\right) = A(x_t - H(x_m)) \quad . \quad (3)$$

where H is an operator to calculate CO layers from the model profiles on the vertical grid of the apriori. Using this observation operator, we remove the influence of the a-priori profile in the calculation of the departures, but knowledge of the a-priori profile is still needed in the observation operator calculations for IASI and MOPITT TCCO retrievals.

A variational bias correction (VarBC) scheme (Dee and Uppala, 2009), where biases are estimated during the analysis by including bias parameters in the control vector, is used for the TCCO IASI data. In this scheme, the bias corrections are continuously adjusted to optimize the consistency with all information used in the analysis. VarBC is applied to the IASI TCCO data, with three predictors: (1) the thickness of the 1000-300 hPa layer, (2) the thermal contrast between the surface temperature and the temperature of the lowest model level over land, and (3) a global constant. MOPITT TCCO data are used to 'anchor' the bias correction, i.e., are assimilated without bias correction. Experience has shown that it is important to anchor the variational bias correction scheme, to avoid drifts in the model fields (Inness et al., 2013). MOPITT is used as the anchor for 'historical' reasons. It was the first instrument assimilated in the early CAMS system, and the assimilation of IASI CO was added later.

The CAMS NRT model and data assimilation system is continually improved as the NWP model and the chemical scheme are further developed and new satellite data are added. Table 2 lists the model upgrades that were implemented during the period discussed in this paper. The change to model CY46R1 on 2021-07-09 had a big impact on the CO analysis field and led to increased negative biases (see Fig. 3 below), likely to be linked to the change of the emission inventories.

In the CAMS 4D-var data assimilation system, the background error covariance matrix is given in a wavelet formulation (Fisher, 2004, 2006). This allows both spatial and spectral variations of the background error covariances. The background errors for CO used in model cycles CY46R1-CY47R2 (OLDBGE) were calculated using the National Meteorological Center (NMC) method (Parrish and Derber, 1992). For this, 150 days of 2-day IFS forecasts (using a 137L configuration of CY45R1) were run, and differences between pairs of 24- and 48-hour forecast fields were calculated whose statistical characteristics serve as proxy for the background errors. For model CY47R3 new CO background errors were calculated (NEWBGE), again with the NMC method, but with a newer model configuration (CY47R1), again using 150 days of 2-day forecasts.

Figure 1 shows the globally averaged vertical CO background error standard deviation profiles and the horizontal correlation profiles from NEWBGE and OLDBGE. NEWBGE standard deviation values are smaller than OLDBGE ones in the troposphere below model level 80 (about 260 hPa) and larger between model levels 80 and 65 (about 260 - 130 hPa). This means that tropospheric CO increments will be smaller with NEWBGE (assuming the data and all other model settings are the same), as the background is penalized less in the 4D-var analysis with NEWBGE than with OLDBGE. The global mean horizontal correlations are longer for NEWBGE than OLDBGE in the boundary layer (below model level 120, about 920 hPa), but shorter above. The horizontal correlations are longest over the continents at the surface, in the Tropics in the free troposphere, and in mid-latitudes around 200 hPa (not shown). The CO background errors are univariate, i.e., the error

https://doi.org/10.5194/acp-2022-458
Preprint. Discussion started: 4 July 2022

Atmospheric Chemistry and Physics Discussions

covariance matrix between CO and other chemical species or dynamical fields is diagonal. They are also constant in time, and globally averaged vertical background error standard deviation profiles are used in the 4D-var procedure.

Table 2: CAMS model cycles used between November 2018 and December 2021 and changes relevant for CO. The horizontal resolution of the global CAMS model was Tl511 throughout the period. More details about model upgrades can be found on https://confluence.ecmwf.int/display/CKB/CAMS%3A+Global+atmospheric+composition+forecast+data+documentation#CAMS:Globalatmosphericcompositionforecastdatadocumentation-EvolutionoftheCAMSglobalforecastingsystem).

In operation from	Model cycle	Model changes affecting CO
2018-06-26	CY45R1	Using MACCity (anthropogenic) and MEGAN_MACC (biogenic) emissions Super-obbing used with sobmin=1, no separate super-obbing for clear and cloudy data
2019-07-09	CY46R1	Vertical resolution change from 60L to 137L, including new background errors for 137L **New emissions inventories**: CAMS_GLOB_ANT v2.1 (anthropogenic) and CAMS_GLOB_BIO v1.1 (biogenic) Biomass-burning injection heights from GFAS used and updated diurnal cycle Online calculation of dry deposition velocities for trace gases Updates to wet deposition parameterisations Updates to chemical reaction rates Super-obbing used with sobmin=6, separate super-obbing for clear and cloudy data
2020-10-06	CY47R1	Updated emissions inventories: CAMS_GLOB_ANT v4.2 (anthropogenic) Update to GFASv1.4 biomass-burning emissions Excluded agricultural waste burning from CAMS_GLOB_ANT, avoiding double-counting with GFAS Super-obbing used with sobmin=1, separate super-obbing for clear and cloudy data
2021-05-18	CY47R2	None
2021-10-12	CY47R3	Updated background error statistics

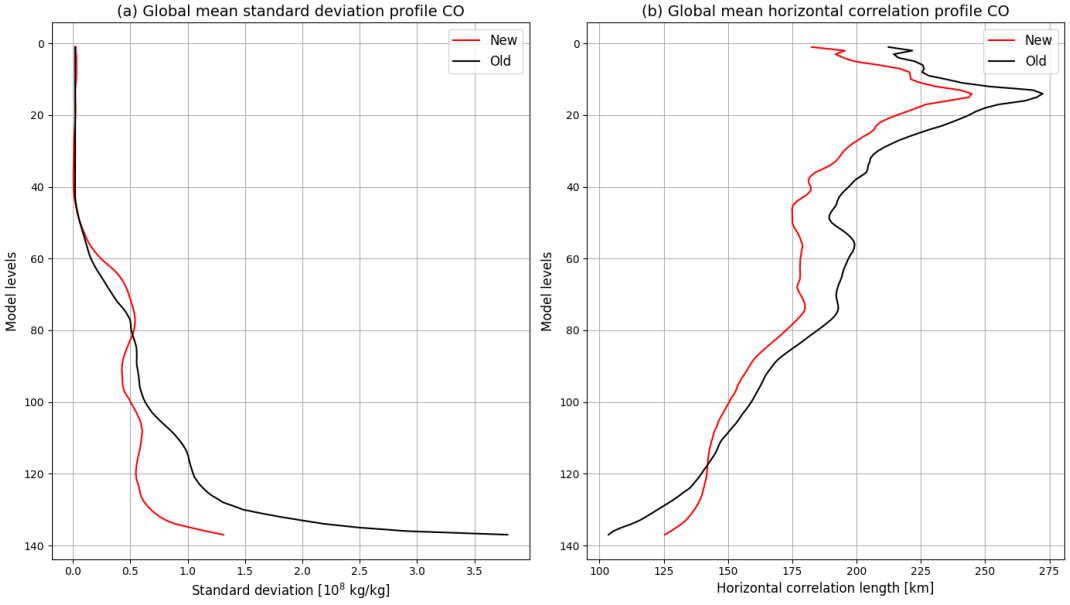

https://doi.org/10.5194/acp-2022-458
Preprint. Discussion started: 4 July 2022

Atmospheric Chemistry and Physics Discussions

Figure 1: Profiles of globally averaged CO (a) background error standard deviation and (b) horizontal background error correlation profiles used from CY46R1 to CY47R2 (black, OLDBGE) and in CY47R3 (red, NEWBGE Model level 137 is the surface, model level 1 the top of the atmosphere and model 60 around 100 hPa.

2.1.2 Quality of CAMS CO analysis fields

CAMS NRT data are routinely validated, and validation reports are produced every three months (https://atmosphere.copernicus.eu/global-services, e.g., Errera et al., 2021). These reports show that the seasonality of the CO field is reproduced well by the global CAMS NRT system, i.e., currently still without the assimilation of TROPOMI data, when compared with independent data. However, the CAMS CO data generally have a negative bias. Compared to IAGOS aircraft CO data the NRT CAMS data show the largest underestimations in the lower troposphere, while upper layers show a better agreement. On average, the modified normalised mean biases (MNMB) with respect to IAGOS CO range between -10% and 5% while correlations are mostly between 40 and 60% (e.g., Errera et al., 2021). Figure 2 shows profiles of seasonal mean relative differences between CAMS profiles and IAGOS (In-service Aircraft for a Global Observing System, www.iagos.org) CO profiles (Nedelec et al., 2003) at Frankfurt airport and averaged over airports in the Eastern United States. These airports were chosen because they had the best data coverage for the period discussed in this paper. Figure 2 shows that the largest relative errors are found in the lower troposphere, with negative biases between -15% and -25% in all seasons. Differences above 700 hPa vary between -5% and -15%. Comparisons with IAGOS cruise level data given in the CAMS validation reports showed mostly negative biases for CAMS data in September, October, November (SON) and March, April, May (MAM) 2021, and no systematic biases in June, July, August (JJA) 2021 and December, January, February (DJF) 2020/2021 when positive and negative biases within ±20% were found in most regions (Errera et al., 2021).

Errera et al., (2021) documents that biases against GAW CO surface observations are within -8% for European GAW stations and Asian stations, and around -16% for stations located in the Southern Hemisphere. Their comparisons with EEA Airbase surface observations in Europe shows high temporal correlations, small biases over Belgium, Germany, Austria, Switzerland, and larger negative biases Spain (-30%), Estonia (-30%), Poland (-50%), the Czech Republic (-60%) and Bulgaria (-65%).

Compared to NDACC FTIR tropospheric column CO data (Figure 3) the CAMS NRT system underestimates the tropospheric CO column in the Northern Hemisphere (NH). This negative bias increased in July 2019 after the CAMS model upgrade to CY46R1 to between -3 to -15 % for most station and is larger than the reported 3% measurement uncertainty. Compared with MOPITT and IASI TCCO data, the CAMS validation reports (e.g., Errera et al., 2021) find negative biases of up to -20% and -30% respectively. These also increased after the CAMS model upgrade to CY46R1 in July 2019. The negative CO bias of the CAMS model is even more pronounced in experiments without CO data assimilation (Errera et al., 2021).

https://doi.org/10.5194/acp-2022-458
Preprint. Discussion started: 4 July 2022

Atmospheric Chemistry and Physics Discussions

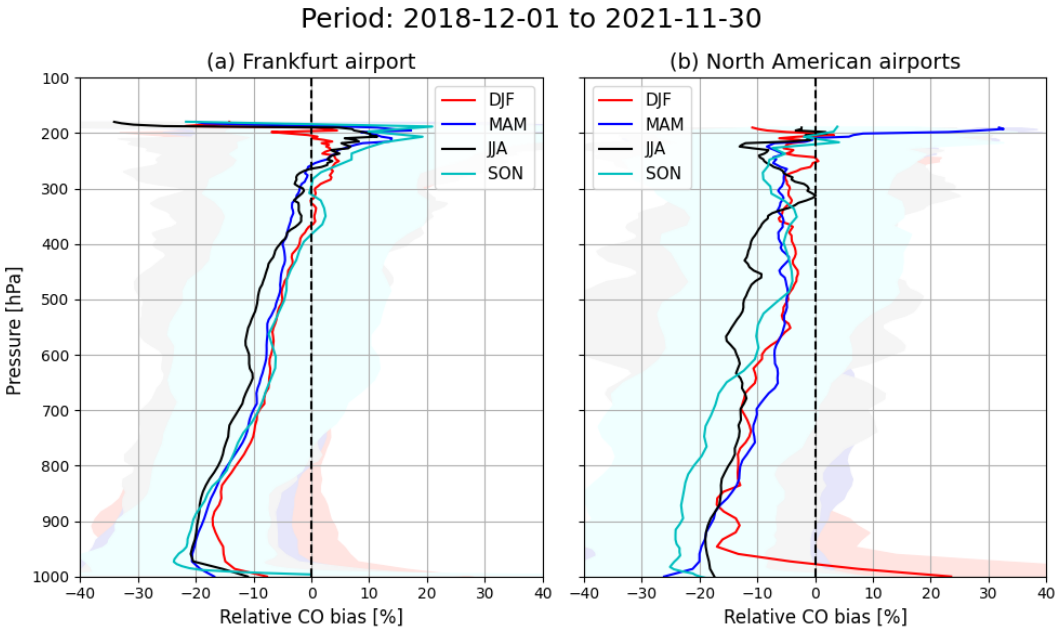

Figure 2: Seasonal mean relative CO biases (%) from the CAMS NRT analysis against IAGOS aircraft data at (a) Frankfurt airport and (b) averaged over North American airports. Shown are (model - observation)/observation*100 for December, January, February (DJF), March, April, May (MAM), June, July, August (JJA) and September, October, November (SON) during the period 2018-12-01 to 2021-11-30. The shaded areas denote ± 1 standard deviation.

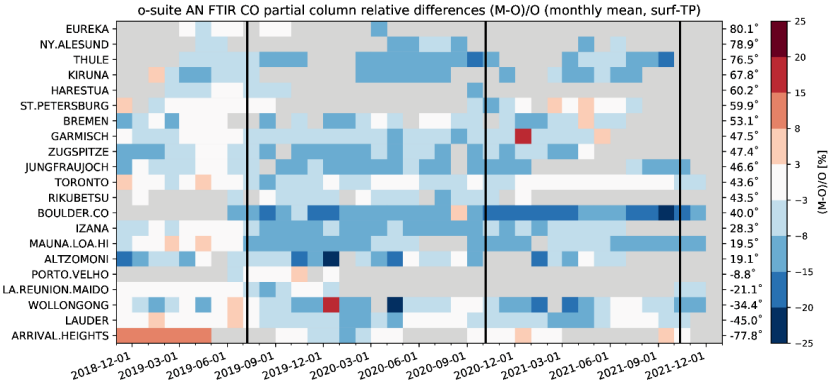

Figure 3: Timeseries of monthly mean relative bias (%) for CAMS CO against NDACC FTIR tropospheric columns. The overall uncertainty for NDACC tropospheric columns is approximately 3%. The stations are sorted by latitude (northern to southern hemisphere). Periods without data are shaded in grey. The FTIR averaging kernels were applied in the comparisons.

2.2 TROPOMI TCCO data

The monitoring of TROPOMI TCCO data in the global CAMS NRT system began on 19 November 2018. TROPOMI has a local overpass time of 13:30 UTC, a spatial resolution of 5.5 km x 7 km in nadir (7 km x 7 km before 6 August 2019) for data retrieved from the SWIR band, a swath of 2600 km and provides daily global coverage with 14 orbits per day. For the work in this paper, we use NRT TROPOMI TCCO data produced with a retrieval algorithm developed by SRON, the Netherlands Institute for Space Research, and provided by ESA/ Eumetsat for the period 19 November 2018 to 31 December 2021. These NRT data are usually available with 3 hours of the observations being taken. Information about updates to the TROPOMI CO retrieval algorithm since November 2018 is given in Table 3.

https://doi.org/10.5194/acp-2022-458
Preprint. Discussion started: 4 July 2022

Atmospheric Chemistry and Physics Discussions

Table 3: TROPOMI algorithm upgrades (from TROPOMI readme file https://sentinels.copernicus.eu/web/sentinel/user-guides/sentinel-5p-tropomi/document-library)

In operation from	Processor Version	Relevant improvements of TROPOMI CO retrieval
2018-11-22	01.02.00	Adjusted qa_value in case of eclipse
2018-12-05	01.02.02	Sun glint was wrongly considered in the qa_value calculation in previous versions
2019-03-27	01.03.00	Added new variables: eastward_wind and northward_wind
2019-04-30	01.03.01	None
2019-08-06		TROPOMI resolution upgrade (for SWIR: 7 km x 7 km before, 5.5 km x 7 km after)
2019-07-03	01.03.02	Offline and NRTI processing chains employ the same algorithm since this Version
2020-12-02	01.04.00	None
2021-07-05	02.02.00	Update CH_4, CO and H_2O cross sections in the CO and CH_4 processors. CO de-striping algorithm for offline data. Improved L1b v2.0 data products
2021-11-17	02.03.01	None

The TROPOMI TCCO retrieval is documented in Landgraf et al. (2016). The retrieval works in the 2.3 μm spectral range of the SWIR part of the solar spectrum (2315-2338 nm) and retrieves the TCCO values for clear-sky and cloudy conditions over land, and for cloudy conditions over ocean. Under clear-sky conditions over oceans, the SWIR signal is too low due to the dark sea surface to give a meaningful retrieval. While TIR measurements like MOPITT and IASI are mostly sensitive to CO in the mid troposphere (Deeter et al., 2013), TROPOMI SWIR measurements are sensitive to the integrated amount of CO along the light path (Landgraf et al., 2016), including the contribution of the planetary boundary layer, making them particularly suitable for detecting surface sources of CO. Martinez-Alonso et al. (2020, their Figure 1) show examples of TROPOMI and MOPITT averaging kernels that illustrate the different sensitivities of the TROPOMI and MOPITT retrievals. Since the update to v01.03.02 on 2019-07-03 the NRT TROPOMI data are of the same quality as the offline retrieval.

The operational TROPOMI CO retrieval deploys a profile scaling approach described in detail by Borsdorff et al. (2014) where a CO reference profile is scaled to fit the TROPOMI reflectance measurements. For this, global, monthly averaged (3° × 2°) vertical CO a-priori profiles from the chemical transport model TM5 (Krol et al., 2005) are used. The forward calculation of the measurement is accounting for light scattering by clouds and aerosols in the atmosphere and thus simultaneously retrieves trace gas columns and effective parameters describing the cloud contamination of the measurements (height scattering layer, scattering optical thickness) as demonstrated by Vidot et al. (2012). The TROPOMI TCCO datasets contain total column averaging kernels for individual measurements that describe the vertical sensitivity of the retrieved CO columns. The CO retrieval under clear-sky atmospheric condition shows a good sensitivity throughout the atmosphere with minor variations due to the observation geometry of the satellite. Retrievals from cloudy measurements exhibit a reduced vertical sensitivity caused by shielding of the cloud in the observation geometry of the satellite. Figure 4 shows examples of TROPOMI averaging kernels for clear-sky and cloudy data over land as well as for cloudy data over sea for the NH, Tropics and SH averaged over the period 2018-11-19 to 2021-12-31 and illustrates the different vertical sensitivities.

Because the TROPOMI CO retrieval is based on the profile scaling inversion (Borsdorff et al., 2014) the total column averaging kernel A_{S5p} cannot smooth the vertical CO a-priori profile that is used for scaling within the inversion, and the validation

https://doi.org/10.5194/acp-2022-458
Preprint. Discussion started: 4 July 2022

Atmospheric Chemistry and Physics Discussions

equation (Eq. 2) simplifies to $y = A_{S5p}\, x_{true}$, where x_{true} is the true CO profile. This means that the CAMS model equivalent of the TROPOMI observations can be calculated as

$$x_{S5P} = A_{S5P}\ x_{mod} = A_{S5P}\, H(x_m) \qquad (4)$$

where x_{mod} is the CAMS model profile on the vertical grid of the TROPOMI a-priori, A_{S5P} the TROPOMI total column averaging kernel and x_{S5P} the resulting CAMS CO column smoothed by the TROPOMI total averaging kernel A_{S5P}.

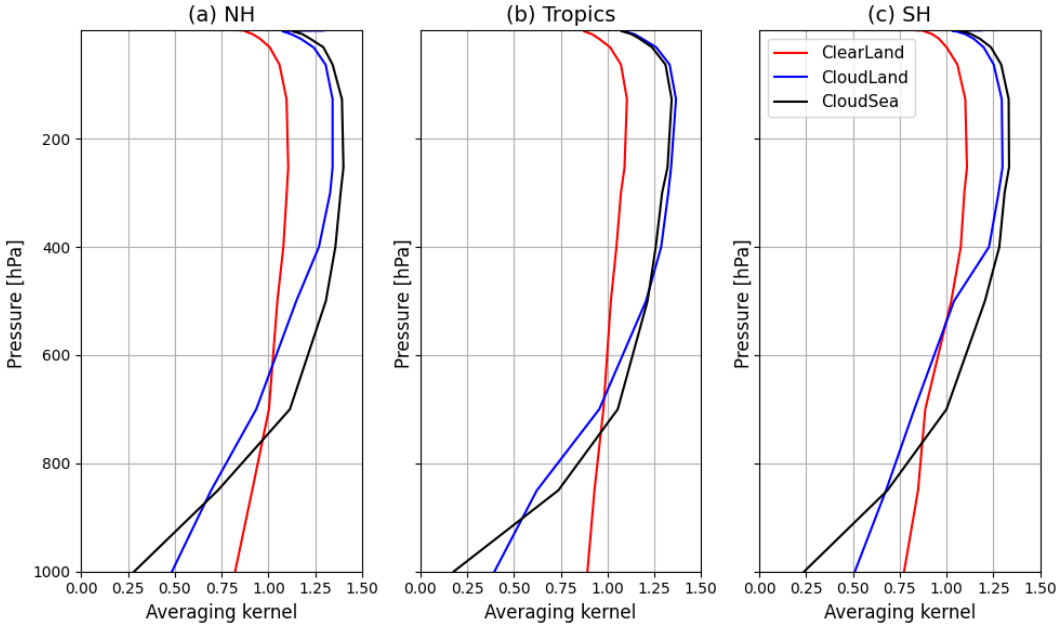

Figure 4: TROPOMI averaging kernels (means for period 2018-11-19 to 2021-12-31) averaged over (a) NH, (b) Tropics and (c) SH for clear data over land (red), cloudy data over land (blue) and cloudy data over sea (black).

As recommended in the TROPOMI readme file (https://sentinels.copernicus.eu/documents/247904/3541451/Sentinel-5P-Carbon-Monoxide-Level-2-Product-Readme-File, last access 2/3/2022), we only use data with quality assurance values (qa_values) >0.5. This filters out the two most westward pixels (because of unresolved calibration issues) and observations with SZA < 80° (where the retrieval is most sensitive to radiometric and retrieval errors due to the long light path through the atmosphere). Furthermore, we separate the data into clear-sky (i.e., clear-sky and clear-sky equivalent) and cloudy pixels. Clear-sky and cloudy data are used over land, while only cloudy data are used over oceans, as in the SWIR clear-sky observations over water have too low signal intensities to be meaningful.

First TROPOMI total column CO (TCCO) data produced with the operational algorithm by SRON showed good agreement with the CAMS NRT CO analysis (Borsdorff et al., 2018) with a mean difference between the data sets of 3.2±5.5 % and a correlation coefficient of 0.97 for a period in November 2017. Martinez-Alonso (2020) compared TROPOMI TCCO (offline and reprocessed) data for the period November 2017 to March 2019 with MOPITT data and with data from the airborne ATom (Atmospheric Tomography mission) campaign and found that over land TROPOMI CO had a small negative bias compared to MOPITT TIR data (-3.73% ± 11.51%) while they were biased slightly high over water (2.98% ± 15.71%). Compared to ATom data (over water) there was also a positive bias of 3.25% ± 11.46%. Sha et al. (2021) reported a bias of 9.22 ± 3.45% against standard TCCON XCO data and 2.45±3.38% against TCCON unscaled XCO for the period from the start of the

https://doi.org/10.5194/acp-2022-458
Preprint. Discussion started: 4 July 2022

TROPOMI mission to 2020-09-30 using the latest offline and reprocessed versions available at the time. While most stations showed positive biases, negative biases were found for urban stations (e.g., Xianghe, JPL and Pasadena). Sha et al. (2021) found differences of on average 6.5±3.54% against NDACC CO columns. All these differences are within the TROPOMI mission requirements on accuracy (< 15%) and precision (<10%).

The routine quarterly TROPOMI validation reports available from https://mpc-vdaf.tropomi.eu/ (last access 7/3/2022) show that the S5P L2_CO (NRT or RPRO concatenated with OFFL) carbon monoxide total column data is in good overall agreement with co-located measurements from the NDACC and TCCON FTIR monitoring networks. For the period November 2017 to September 2021, TROPOMI offline data had a positive bias of 6.5 % with respect to NDACC data and 9.24% with respect to TCCON data. The validation report found no latitudinal dependence of the bias and a slight increase of the bias during local winter. Larger biases (>15%) were seen with respect to NDACC data from Arrival Height (Antarctica). Most individual TCCON stations had biases below 12%, but biases > 12% were found in the Arctic and at mountain stations. The biases increased with solar zenith angle by about 10% between 10° and 80°. An upper boundary of the random uncertainty of the TROPOMI offline CO data is 5%, according to the validation reports. Individual TROPOMI CO data show stripes of erroneous CO values < 5% in flight direction, probably associated with calibration issues. A de-striping algorithm has been included for offline TROPOMI data with the upgrade to v02.02.02 in July 2021, but this is not applied to the NRT data. TROPOMI also suffers from instrumental effects in the area of the South Atlantic Anomaly (SAA).

According to the TROPOMI product readme file (https://sentinels.copernicus.eu/documents/247904/3541451/Sentinel-5P-Carbon-Monoxide-Level-2-Product-Readme-File.pdf/f8942626-ffb6-4951-90fc-a16b6589e39e?t=1639982223246, last access 27/4/2022) and the validation reports, the TROPOMI NRT CO product (which is used in the global CAMS system and in this paper) had an additional positive bias of 3-4 % before July 2019, but since processor version 01.03.02, the same configuration settings are used for the NRT and offline data processing streams, and therefore the data products are of the same quality. However, there is no noticeable change in the TROPOMI monitoring timeseries (Figures 9 to 11 below) related to the switch to the offline algorithm for NRT data, and in the timeseries of analysis departures this change is masked by the CAMS model change to CY46R1 that happened a few days afterwards.

2.3 TROPOMI super-observations for use in CAMS system

Because the horizontal resolution of the TROPOMI TCCO data (5.5 km x 7 km) is higher than the model resolution of T511 (about 40 km x 40 km) the TROPOMI data are not spatially representative for the model grid boxes. To overcome this representativeness error, the data are converted into so called ‘super-observations’ before they are included in the CAMS system. For this, the data are averaged to the T511 resolution of the model. The averaging is carried out separately for different surface types (e.g., land, ocean, ice etc.) and for clear and cloudy data, and the observation errors and averaging kernels of the data are averaged in the same way as the observations. The super-obbing reduces the random errors in the data.

In the current CAMS configuration (CY47R3, see Table 2), super-observations are created if at least one observation is located in the grid-box. However, due to a coding error, in an early CAMS configuration (CY46R1), which was operational between 2019-07-09 and 2020-10-05 (see Table 2), super-observations were only created if at least 6 observations were found in a grid-box. This led to a reduced number of super-observations during this period (see Fig. 9 to 11 below), and particularly affected data at cloud boundaries, where there are often smaller numbers of data of one type in one grid box. In the model cycle used prior to 2019-07-09 (CY45R1) super-observations were created if at least one observation was available in a grid-box, but the

https://doi.org/10.5194/acp-2022-458
Preprint. Discussion started: 4 July 2022

Atmospheric Chemistry and Physics Discussions

super-observation method did not distinguish between clear and cloudy data. This was later corrected. These changes explain the differences in the number of data displayed in the monitoring timeseries in Fig. 9 to 11 below.

3 Monitoring of TROPOMI NRT data with the CAMS DA system

Figure 5 shows maps of seasonal mean TROPOM CO columns between December 2018 and November 2021. CO values are generally higher in the NH than in the SH, except in the biomass burning regions in the tropics. This reflects the greater anthropogenic emissions in the NH (e.g., Fortems-Cheiney, 2011). Values in the NH are highest during winter and spring, largely due to the lower concentrations of the OH radical during winter, which is the major sink for CO. The largest NH TCCO values are found over southeast Asia in DJF and MAM, and transport of CO rich air from southeast Asia and North America eastwards by the prevailing winds leads to high CO columns over the North Pacific and North Atlantic, respectively. Minimum values in the NH are found in JJA except in areas affected by boreal wildfires (e.g., Siberia, Northern America). CO from biomass burning in the tropics has a different seasonality. In Africa, maximum CO columns are seen north of the equator in DJF, when biomass burning takes place in the Sahel region and equatorial West Africa during the local dry season. In MAM the fire signal over Africa is weaker, and by JJA the affected area has moved south of the equator. In SON the signal is weaker than in JJA but extends further to the south and east. It generally peaks in August, but the season extends to November. In South America the strongest biomass burning signal is seen in SON. Here, deforestation fires and agricultural fires occur south of 10˚S during August–October with a peak in September.

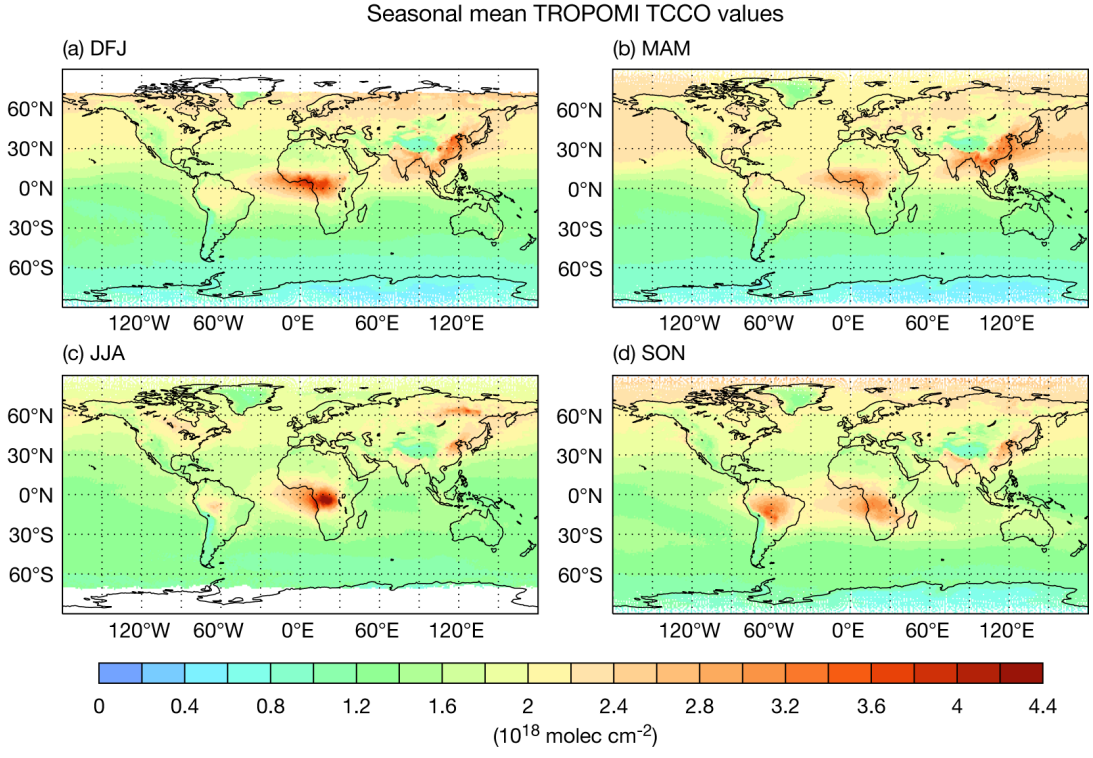

Figure 5: Maps of seasonal mean TROPOMI CO columns in 10^{18} molec/cm^2 for (a) DJF, (b) MAM, (c) JJA and (d) SON for the period December 2018 to November 2021. Shown are all 'good' values, i.e., all observations given qa_value >0.5 by the data providers.

https://doi.org/10.5194/acp-2022-458
Preprint. Discussion started: 4 July 2022

Atmospheric Chemistry and Physics Discussions

Figure 6 shows the seasonal mean differences between TROPOMI TCCO observation values and CAMS analysis fields. The TROPOMI averaging kernels were applied to the CAMS model profiles in the calculation. The differences are positive everywhere except in a small area over Indonesia in SON, which is affected by biomass burning. The largest absolute differences are found at high latitudes in the NH in DJF, and over SE Asia, as well as over tropical Africa in DJF and JJA. We also see large differences over sea in the area of the South Atlantic Anomaly. These were traced back to observations with qa_value=1 but marked as clear-sky. In these cases, the forward model assumes a cloud free atmosphere which makes no sense over oceans due to the low reflectivity of water in the SWIR. We have excluded these observations in the assimilation experiment discussed in Section 4 below.

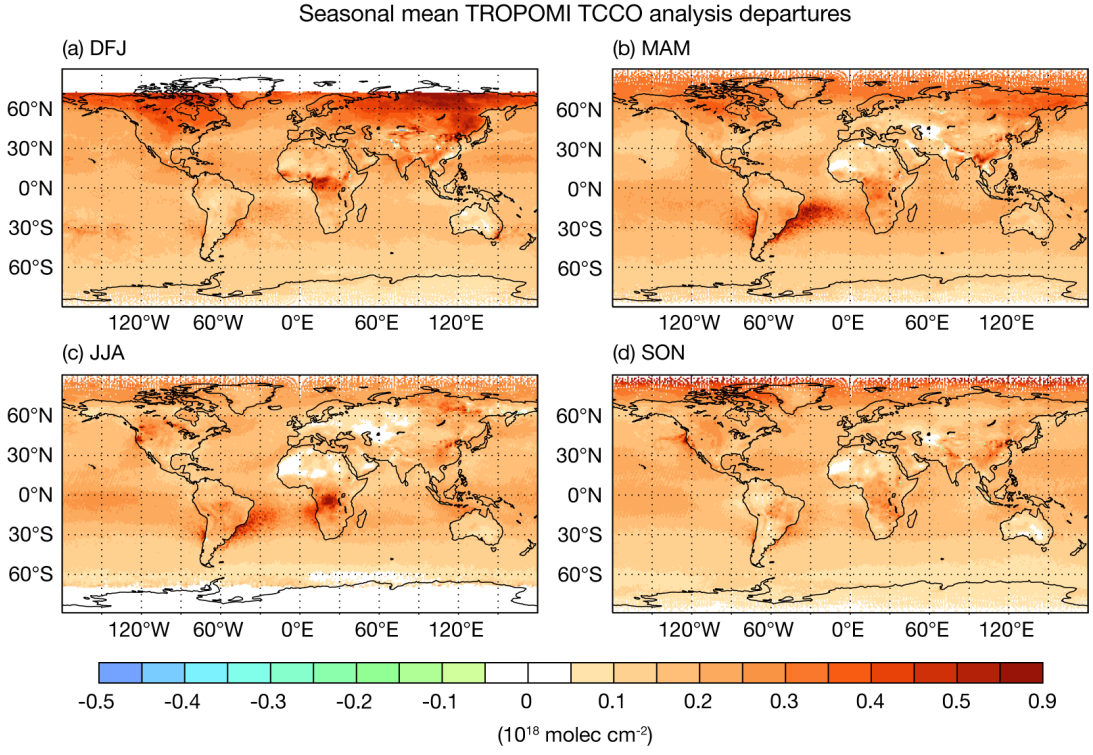

Figure 6: Seasonal mean maps of TROPOMI CO analysis departures in 10^{18} molec/cm^2 for (a) DJF, (b) MAM, (c) JJA and (d) SON for the period December 2018 to November 2021. Shown are all 'good' values, i.e., all observations given qa_value>0.5 by the data providers.

Figure 7 shows boxplots of relative differences between TROPOMI TCCO and CAMS analysis values for the various latitude bands for the period 2018-11-19 to 2021-12-31. Averaged over the globe the median analysis departures are of the order 9-11%, with the smallest departures (medium value of 9.4%) seen for cloudy data over land and the largest departures (10.7%) over sea. In the polar latitude bands, i.e., the areas where no satellite data are assimilated in the CAMS system, the analysis departures are largest (11-14%). In NH midlatitude (60-30ºN) the largest departures are found for clear data over land (10.5 %), while cloudy data over land have smaller departures (9.3 %), and the smallest departures in this latitude band is found over sea (8.4 %). In the Tropics the largest analysis departures are found over sea (11.0 %) while values over land have a median of 8.8 % for cloudy observations and 6.6 % for clear-sky observations. In the SH mid-latitudes, the smallest median analysis departures are also found for clear-sky data over land (8.9 %) and the largest ones over sea (10.7 %).

https://doi.org/10.5194/acp-2022-458
Preprint. Discussion started: 4 July 2022

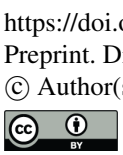

Atmospheric Chemistry and Physics Discussions

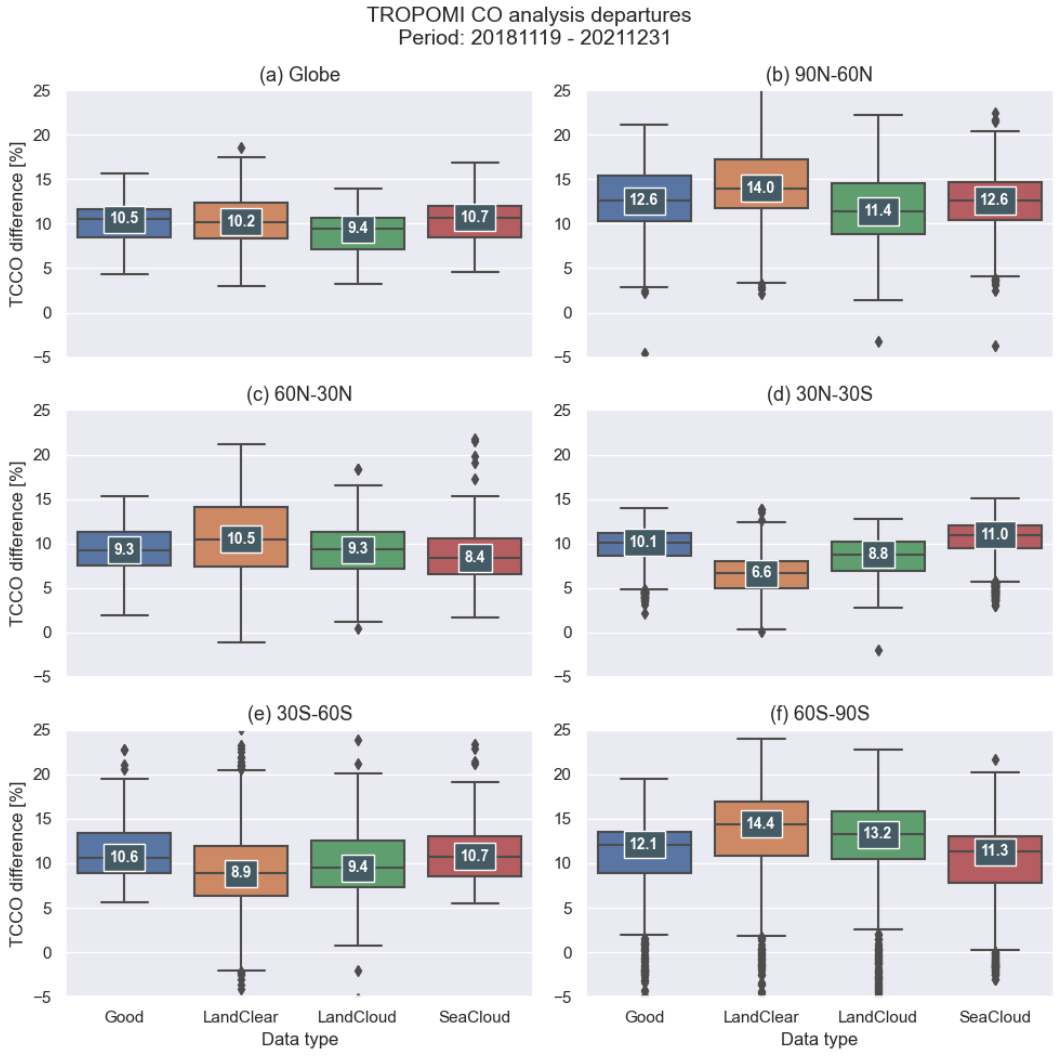

Figure 7: Boxplot of relative differences between TROPOMI TCCO observation and CAMS values values in % for the period 2018-11-19 to 2021-12-31 and the areas: (a) Globe, (b) 90-60˚N, (c) 60-30˚N, (d) 30˚N-30˚S, (e) 30-60˚S and (f) 60-90˚S. The box extends from the first (Q1) to the third (Q3) quartile values of the data, with a line at the median (Q2). The whiskers extend from the edges of box to show the range of the data. By default, they extend no more than 1.5 * IQR (IQR = Q3 - Q1) from the edges of the box, ending at the farthest data point within that interval. Outliers are plotted as separate dots. 'Good' data are all TROPOMI pixels given qa_values >0.5 by the data providers.

Figure 8 shows timeseries of the global mean daily analysis departures, observation values, standard deviation of observations and number of observations for TROPOMI TCCO in the NRT CAMS system for the period 2018-11-19 to 2021-12-31. The TROPOMI TCCO data were monitored passively during this period, i.e., not used in the analysis, and therefore have no impact on the CAMS CO fields. The timeseries of the analysis departures is affected by model upgrades (see Table 2) as well as by TROPOMI retrieval algorithm upgrades (see Table 3), while the timeseries of the observations and standard deviation of observations are only affected by changes to the TROPOMI retrieval algorithm. The changes in TROPOMI data numbers in July 2019 and October 2020 come from the changes to the settings for creating the super-observations (discussed in section 2.3) and not from changes to the TROPOMI NRT data delivery. However, there is no noticeable impact from this change on the analysis departures and observation values. A small increase in data numbers is seen in August 2019 when the TROPOMI

https://doi.org/10.5194/acp-2022-458
Preprint. Discussion started: 4 July 2022

Atmospheric Chemistry and Physics Discussions

horizontal resolution was increased from 7 km x 7 km to 5.5 km x 7 km, but this increase is small, because TROPOMI data were already used at a resolution of T511 in the CAMS system. Separate timeseries are shown in Fig. 8 for good data (i.e., all observations with qa_values >0.5), clear and cloudy data over land, and cloudy data over sea. The analysis departures are positive throughout the time period, denoting that TROPOMI TCCO data are always larger than the CAMS analysis values. This agrees with the negative bias of the CAMS CO data that is documented in the routine CAMS evaluation reports (e.g., Errera, et al., 2021). The timeseries show a change to increased departures in July 2019 (from relative differences between 5-10% for 'good' data before July 2019 to 10-15% afterwards). Such an increase is not seen in the observation timeseries and is related to the CAMS model upgrade to CY46R1. This model upgrade included a change to the anthropogenic and biogenic emission data sets used in the CAMS NRT system (from MACCity and MEGAN_MACC prior to July 2019 to CAMS_GLOB_ANT and CAMS_BLOB_BIO afterwards). This change led to lower CAMS CO values and an increased negative bias relative to independent observations, as seen in Fig. 3, and was also reported in the quarterly CAMS evaluation reports on https://atmosphere.copernicus.eu/eqa-reports-global-services (e.g. Errera et al., 2021). The other changes listed in Tables 2 and 3 had smaller impacts on the global TCCO field, but there is a change after the TROPOMI algorithm upgrade in July 2021 leading to lower analysis departures, and after the CAMS upgrade to CY47R3 in October 2021 after which the global mean analysis departures for all observation types are below about 8%. The TROPOMI upgrade in July 2021 included an upgrade to the CO and CH_4 cross sections used in the retrieval. It is possible that the better fit of the methane absorption gives better cloud parameters and hence a better estimation of the vertical sensitivity.

The timeseries of the observation values and the departures show clear differences between the TROPOMI observations over land and sea (to be expected as they cover different areas), and also pronounced differences between the clear-sky and cloudy data over land the origin of which is not yet clear. The timeseries of the observation standard deviation shows several spikes during NH summers related to boreal wildfires that emit large amounts of CO into the atmosphere (Witze 2020; https://atmosphere.copernicus.eu/copernicus-reveals-summer-2020s-arctic-wildfires-set-new-emission-records). The spike seen in Fig. 6 in January 2020 is related to large Australian bushfires in 2019/2020 (Li et al., 2020; Ohneiser, 2020; Pope et al., 2021; John et al., 2021; van der Velde et al., 2021).

https://doi.org/10.5194/acp-2022-458
Preprint. Discussion started: 4 July 2022

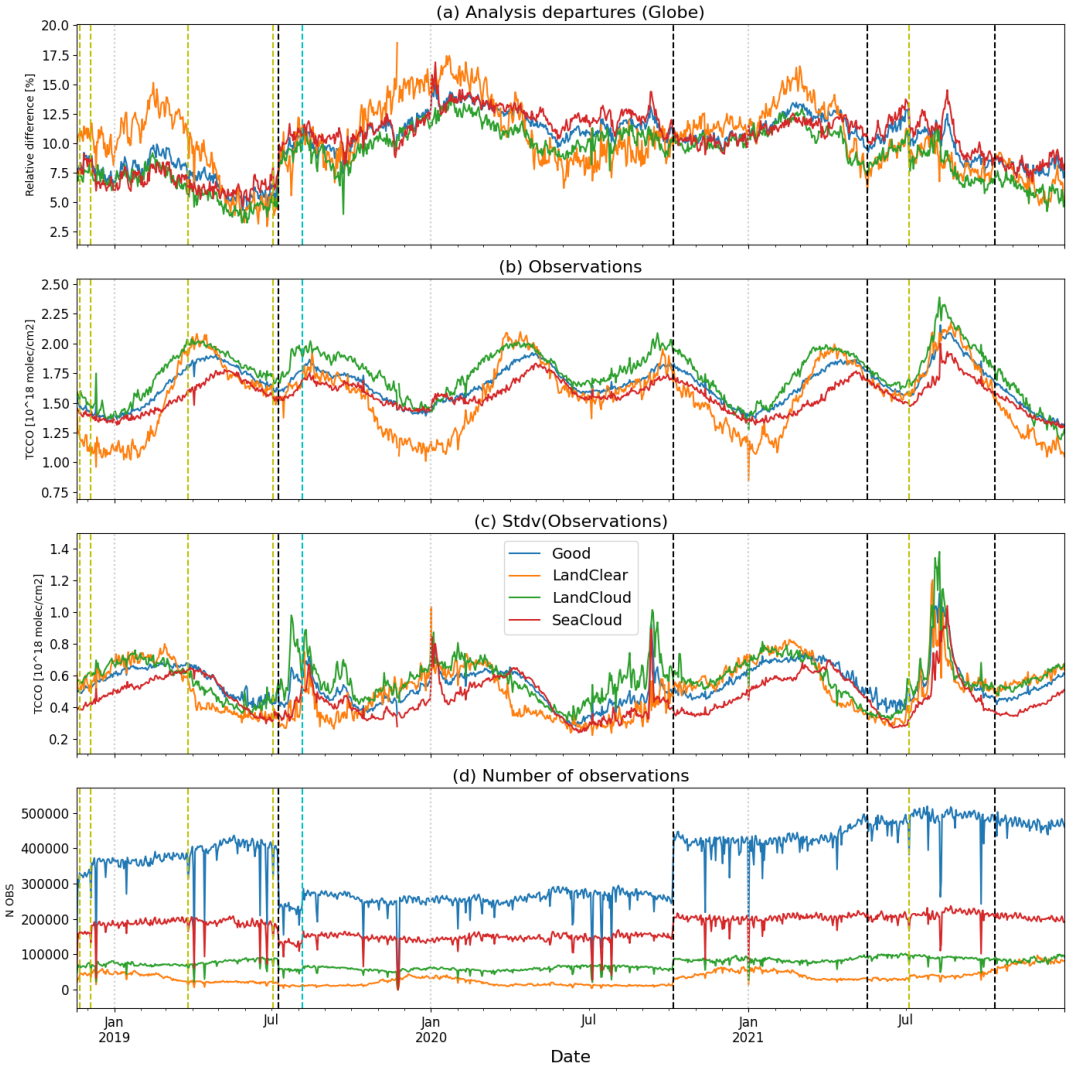

Figure 8: Timeseries of daily mean global mean TROPOMI TCCO (a) analysis departures (in %), (b) observations (in 10^{18} molec/cm^2), (c) standard deviation of observations (in 10^{18} molec/cm^2) and (d) number of observations for the period 2018-11-19 to 2021-12-31. Vertical dashed black lines mark IFS model upgrades (see Table 2), yellow lines TROPOMI algorithm upgrades (see Table 3), the cyan line the TROPOMI horizontal resolution upgrade on 2019-08-06 and the grey dotted lines the year changes.

As already discussed in Section 2.1, CAMS validation reports show negative biases for tropospheric CO against NDACC FTIR data of about -5 to -15 % after the change to 46R1 in July 2019 and -5 to -10 % against TCCON data, as well as negative biases with respect to MOPITT (-5 to -10 %) and IASI (-10 to -30 %). Figure 3 also shows the negative bias in CAMS TCCO after the model upgrade in July 2019 of between -3% to -15% with respect to NDACC FTIR data. This suggests that large

https://doi.org/10.5194/acp-2022-458
Preprint. Discussion started: 4 July 2022

parts of the TROPOMI TCCO analysis departures shown in Fig. 7 and 8 are the result of a low bias of the CAMS model, rather than a high bias of the TROPOMI NRT TCCO product.

4 Results of TROPOMI CO assimilation test

4.1 Results from single observation experiments

Before carrying out longer assimilation experiments with the TROPOMI TCCO data, we look at the results of single observation experiments with the data to illustrate the different impact clear and cloudy data have in the analysis, and to highlight the importance of using the averaging kernels in the observation operators. We carry out three single observation experiments. In each one, we place a single TROPOMI observation with a prescribed TCCO value of 4.3 10^{18} molec/cm^2 and observation error of 10% at (50˚N, 10˚E) but vary the averaging kernels of the observations, so they are representative of mid-level cloudy conditions, clear-sky conditions and clear-sky equivalent conditions (i.e., low thin clouds) over land (see Fig. 9). The resulting analysis increment profiles show that the clear-sky and clear-sky equivalent observations have a large impact in the troposphere below 550 hPa, including in the boundary layer. The impact of the cloudy data is reduced in the lower troposphere, i.e., below the clouds, where the averaging kernel values are smaller, and are larger above 500 hPa. If the averaging kernels were not used in the observation operator, e.g., the model equivalents of the observations were calculated as simple vertical integrals, all three experiments would give the same analysis profiles. This illustrates the importance of taking the averaging kernels into account when comparing model data with satellite retrievals.

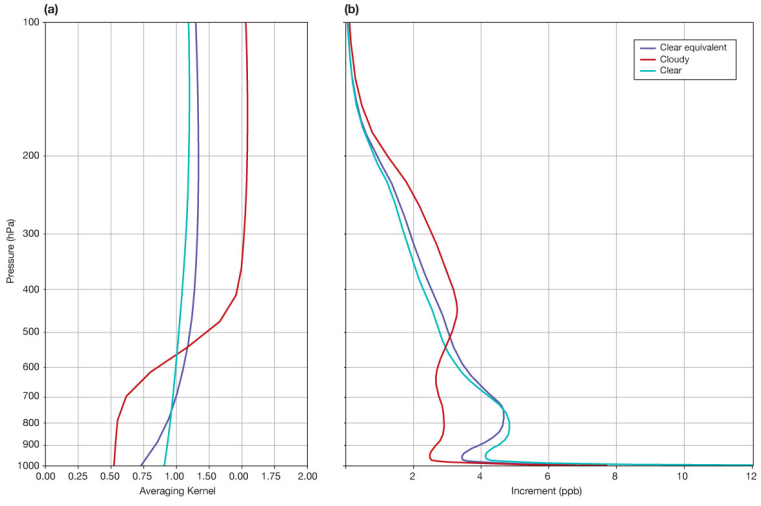

Figure 9: (a) TROPOMI total column averaging kernels representative of cloudy (red), clear-sky (cyan) and clear-sky equivalent (i.e., low thin clouds) conditions (blue) over land. (b) Analysis increments obtained in single observation experiments with the CAMS system using observations with these averaging kernels and prescribed TCCO value of 4.3 10^{18} molec/cm^2 and observation error of 10% located at (50˚N, 10˚E).

4.2 Results from assimilation experiments for the period 2021-07-06 to 2021-12-31

Assimilation tests with the CAMS system were carried out with the TROPOMI TCCO data for the period 2021-07-06 to 2021-12-31, i.e., after the TROPOMI algorithm upgrade to v02.02.00 (see Table 3). In the assimilation experiment (ASSIM, see Table 4) TROPOMI data were used between 90˚N and 60˚S, i.e., not over Antarctica, if they had qa_values>0.5. Over oceans, only cloudy data were used. We also produced a control experiment (CTRL, see Table 4) where TROPOMI data were included passively and not assimilated. The differences between ASSIM and CTRL allow us to assess the impact of the TROPOMI TCCO data on the CAMS CO analysis. The model cycle used for the experiments was CY47R3, meaning that the CTRL setup corresponds to the CAMS NRT configuration that was operational from October 2021. The TROPOMI data in both

https://doi.org/10.5194/acp-2022-458
Preprint. Discussion started: 4 July 2022

experiments were super-obbed to the model resolution of T511, as described in Section 2.3. In ASSIM TROPOMI TCCO is used without bias correction, because the TROPOMI SWIR retrieval has different sensitivity to CO in the atmosphere than the IASI and MOPITT TIR retrievals, and it would not make sense to anchor a bias correction for TROPOMI to MOPITT or IASI.

Table 4: Experiments used for the TROPOMI assimilation tests for the period 2021-07-06 to 2021-12-31.

Experiment name	Expver/ model cycle/ DOI	Assimilated data	Bias correction
ASSIM	hmib (Inness, 2022a) CY47R3 https://doi.org/10.21957/ax0c-fm72	TROPOMI, MOPITT (day & night), IASI-BC (day)	VarBC applied to IASI-BC (see Table 1)
CTRL	hlxm (Inness, 2022b) CY47R3 https://doi.org/10.21957/mwqe-vs95	MOPITT (day & night), IASI-BC (day)	VarBC applied to IASI-BC (see Table 1)

4.2.1 Difference plots ASSIM minus CTRL experiments

Figure 10a shows a map of the relative differences between TCCO fields from ASSIM and CTRL averaged over the period 2021-08-01 to 2021-12-30 and illustrates that the assimilation of TROPOMI TCCO data leads to increased CO columns in the analysis. The largest relative increase is found at high latitudes north of 70˚N (25-30%), over North America (10-20%) and over oceans (10-20%) in the Tropics. Such increases are expected if the CAMS analysis is drawing to the TROPOMI data, considering the positive TROPOMI analysis departures seen in the monitoring plot (Fig. 8) and the generally negative bias of the CAMS CO fields. The large differences north of 70˚N are in the area where no IASI or MOPITT TCCO data are assimilated, i.e., no TCCO at all are assimilated here in CTRL. Figure 10b shows a cross section of the zonal mean absolute differences between ASSIM and CTRL for the same period and illustrates that CO is increased most at the surface and in the lower troposphere in the NH, with differences north of 60˚N extending throughout the troposphere, as well as in the upper troposphere in the Tropics. It is not clear yet if this is the direct result of the assimilation of TROPOMI data leading to increased CO in the upper troposphere, or it could be the result of convective transport. Figure 10c shows the time evolution of the zonal mean relative differences between ASSIM and CTRL and illustrates that the largest differences are found in July and August, i.e., at a time when large boreal wildfires burned in Siberia and North America (see also section 4.2.4 below).

https://doi.org/10.5194/acp-2022-458
Preprint. Discussion started: 4 July 2022

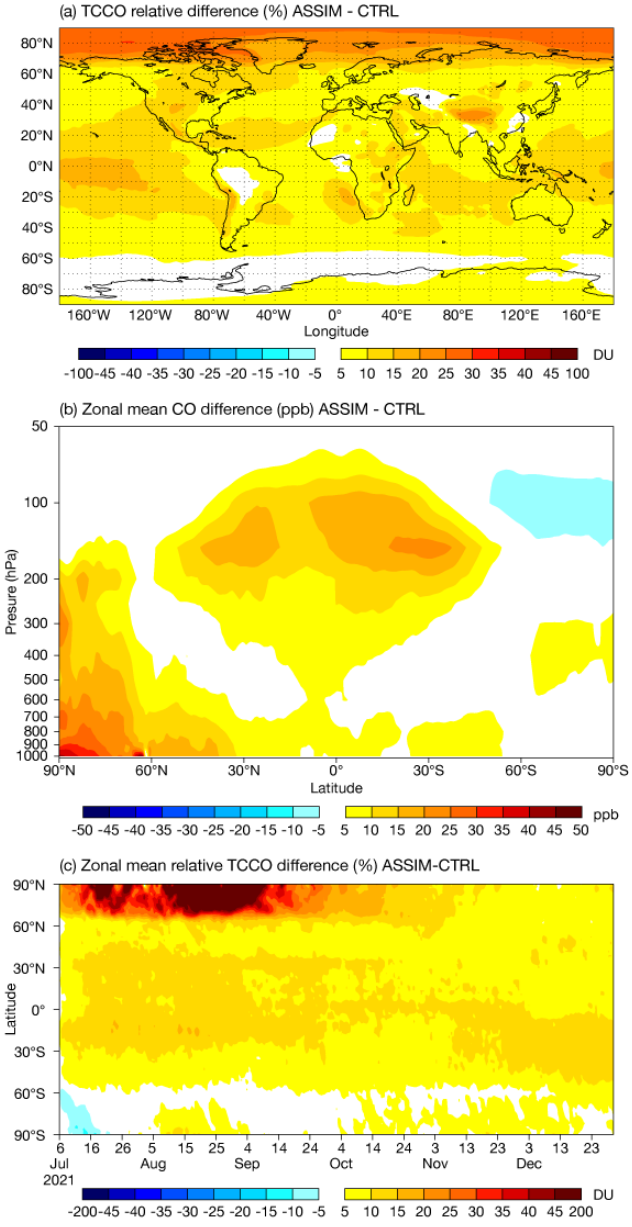

Figure 10: (a) Relative TCCO difference in 10^{18} molec/cm^2 (left), (b) zonal mean cross section of CO difference in ppb from ASSIM minus CTRL averaged over the period August to December 2021 and (c) timeseries of daily zonal mean TCCO relative differences [%] for the period 2021-07-06 to 2021-12-30.

4.2.2 Instrument-specific analysis departures

Next, we look at the fit of the CO analysis to the assimilated CO data in ASSIM and CTRL. Figure 11 shows boxplots of averaged global mean analysis departures from CTRL and ASSIM. In CTRL, TROPOMI analysis departures vary between 7.3% to 9.1%, for the different data types. Analysis departures for MOPITT (0.6 %), IASI-B (1.5%) and IASI-C (1.3%) are much smaller because these data are assimilated, and the analysis is drawing to the data. MOPITT has the smallest analysis departures because the data are assimilated without bias correction. In ASSIM, the analysis is drawing to the TROPOMI data in addition to MOPITT and IASI-BC, so that TROPOMI analysis departures are much reduced and now lie between 0.3 and

https://doi.org/10.5194/acp-2022-458
Preprint. Discussion started: 4 July 2022

Atmospheric Chemistry and Physics Discussions

0.8 % for the various data types. IASI-BC analysis departures are also reduced slightly, illustrating that the assimilation of TROPOMI CO improves the fit of the CAMS analysis to the IASI-BC data globally. MOPITT departures are increased in ASSIM, because MOPITT TCCO values are generally lower than TROPOMI and IASI values, and by assimilating TROPOMI (without bias correction) in addition to the other data products the TCCO analysis values are increased (Fig. 10) and the fit to MOPITT is degraded.

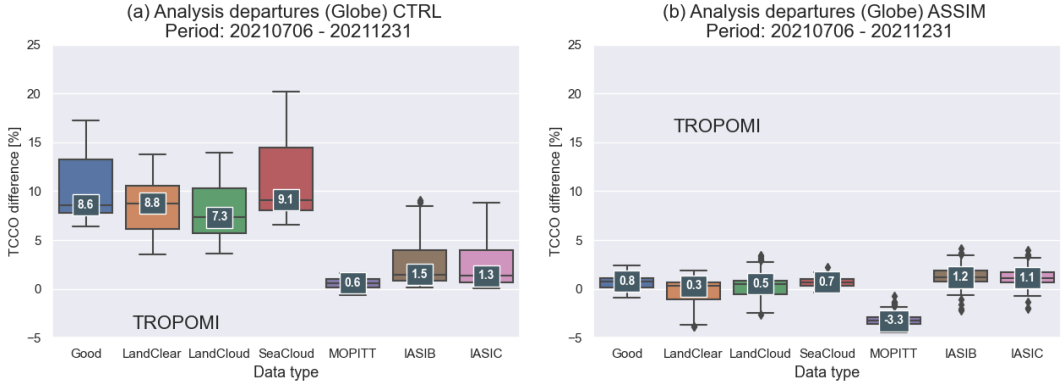

Figure 11: Global mean analysis departures for TROPOMI data (Good, LandClear, LandCloud, SeaCloud) and daytime MOPITT and IASI-BC data averaged over the period 2021-07-06 to 2021-12-31 for (a) CTRL and (b) ASSIM.

Figure 12 shows timeseries of daily mean analysis departures from the four instruments averaged over the area between 60˚N and 60˚S, i.e., excluding the polar regions where the NRT MOPITT product does not provide data. The analysis in ASSIM is drawing strongly to the TROPOMI data (Fig. 12a), and TROPOMI analysis and first-guess departures are much reduced in ASSIM compared to CTRL. IASI-BC analysis departures are also reduced in ASSIM during July and August, and of similar size to the ones in CTRL for the rest of the timeseries. MOPITT departures in ASSIM are more negative than in CTRL (as already seen in Fig. 11b). Figure 13 takes a closer look at the analysis departures in the Arctic from IASI-B and IASI-C. Here we see a much-improved fit in July and August when the high CO columns retrieved by IASI-BC, which are the result of strong boreal wildfires in Siberia and North America, are not well captured in CTRL. The improved fit against IASI-BC in ASSIM continues throughout September and October, i.e., while TROPOMI data are available for assimilation north of 60˚N. They are more similar in both experiments after November, when no TROPOMI data are available for assimilation in this latitude band. Examples of the impact of boreal wildfires in August 2021 on the CAMS TCCO analysis are discussed in Section 4.2.4 below.

https://doi.org/10.5194/acp-2022-458
Preprint. Discussion started: 4 July 2022

Atmospheric Chemistry and Physics Discussions

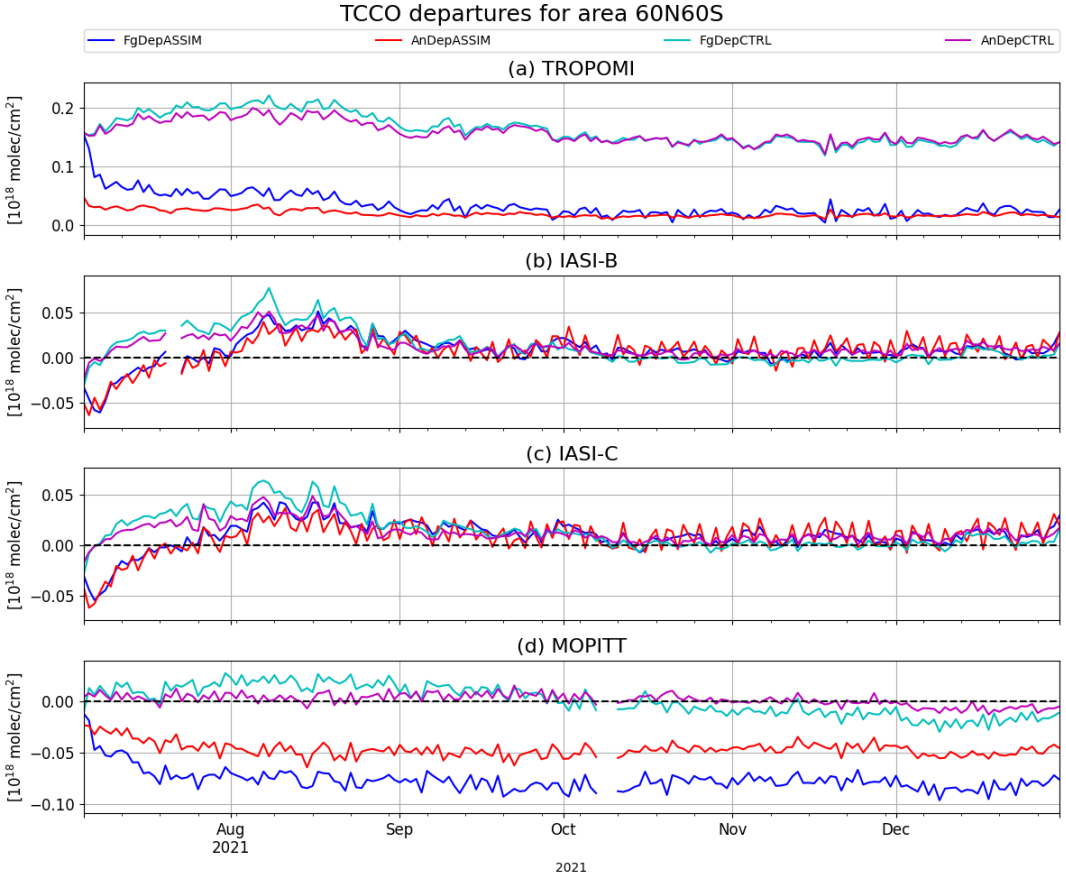

Figure 12: Timeseries from 2021-07-06 to 2021-12-31 of daily mean TCCO first-guess and analysis departures from ASSIM and CTRL for (a) TROPOMI, (b) IASI-B, (c) IASI-C and (d) MOPITT for all 'good data' averaged over between 60ºN-60ºS in 10^{18} molec/cm^2. Analysis departures from ASSIM are in red, for CTRL in magenta. First-guess departures from ASSIM are in blue, for CTRL in black.

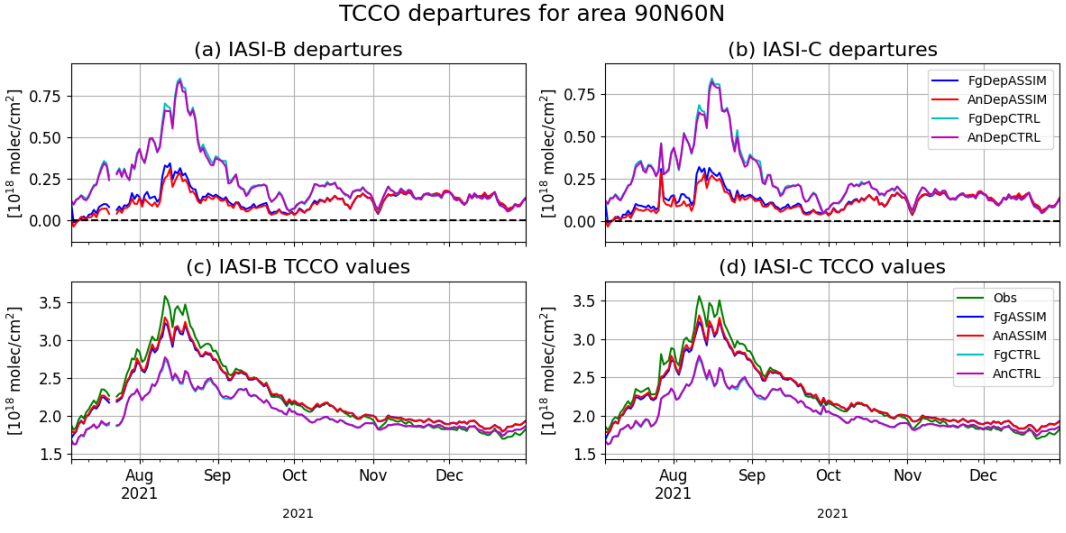

https://doi.org/10.5194/acp-2022-458
Preprint. Discussion started: 4 July 2022

Atmospheric Chemistry and Physics Discussions

Figure 13: Timeseries from 2021-07-06 to 2021-12-31 of daily mean TCCO first-guess and analysis departures from (a) IASI-B and (b) IASI-C, and TCCO values from observations, analysis and first-guess for (c) IASI-B and (d) IASI-C in 10^{18} molec/cm^2 for all 'good data' averaged over the area between 90-60ºN. Analysis departures/ values from ASSIM are in red, for CTRL in magenta. First-guess departures/ values from ASSIM are in blue, for CTRL in black. IASI TCCO values are in green. IASI data are not assimilated north of 65ºN.

4.2.3 Evaluation against independent observations

To assess the quality of the TROPOMI analysis we compare the TCCO fields from ASSIM and CTRL with independent observations, i.e., observations that were not used in the analysis. Figure 14 shows comparison against NDACC FTIR data at all available stations. The negative CO total column and tropospheric column biases seen in CTRL are much reduced in ASSIM everywhere, except at the Antarctic station of Arrivals Heights where ASSIM shows a larger positive bias which increases with time. As no TROPOMI CO data are assimilated south of 60˚S in ASSIM, but the assimilation leads to increased CO values elsewhere, this increase over Antarctica must be the result of transport into the Antarctic region. Stratospheric CO in ASSIM has a reduced bias in the SH, but larger positive biases in the NH and Tropics than in CTR. As the CAMS system only uses a tropospheric chemistry scheme, we do not assess the changes to stratospheric CO any further. Figure 15 shows the mean biases and standard deviation values at each NDACC station for the period 2021-07-06 to 2021-12-31 and confirms the strong reduction of the total and tropospheric column CO biases in ASSIM.

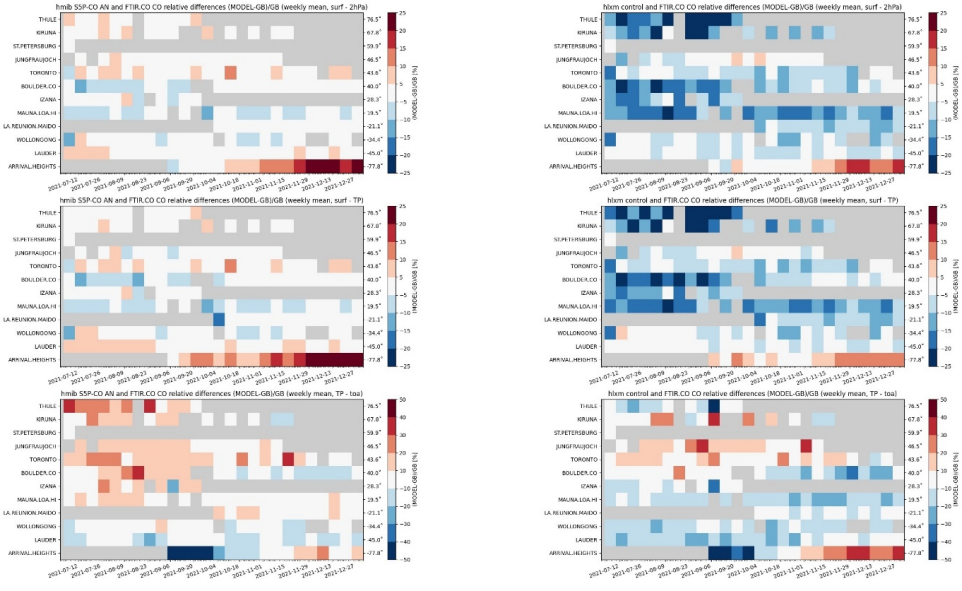

Figure 14: Timeseries of relative mean bias for total column CO (row 1), tropospheric CO columns (row 2) and stratospheric column (row 3) in % from ASSIM (left) and CTRL (right) against NDACC FTIR data for the period 2021-07-06 to 2021-12-31. The overall uncertainty for NDACC tropospheric columns is approximately 3%. The stations are sorted by latitude (northern to southern hemisphere). Periods without data are shaded in grey.

https://doi.org/10.5194/acp-2022-458
Preprint. Discussion started: 4 July 2022

Atmospheric Chemistry and Physics Discussions

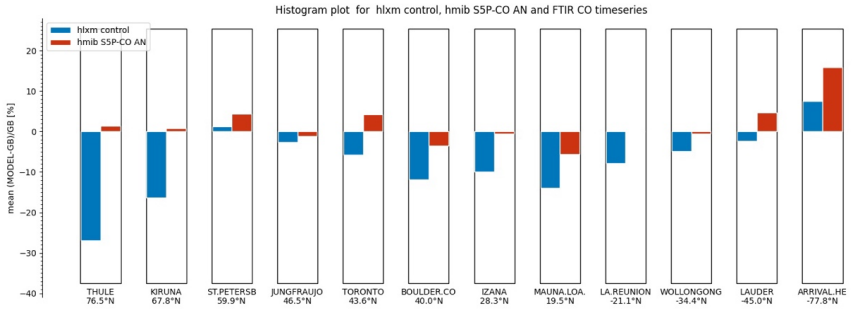

Figure 15: Histogram plot of relative differences in % against NDACC FTIR data tropospheric column CO from ASSIM (red) and CTRL (blue) for the period 2021-07-06 to 2021-12-31. Note that St. Petersburg only had one profile on 2021-07-07.

Figure 16 shows comparisons of tropospheric CO profiles from ASSIM and CTRL with IAGOS aircraft data at various airports averaged over the period July to December 2021, and Figure 17 shows timeseries of the monthly mean MNMB against IAGOS CO for layers in the upper troposphere, mid-troposphere and lower troposphere. We see a clear improvement in ASSIM with reduced biases, particularly in the lower and mid-troposphere at Frankfurt, North American and Middle Eastern airports. Here, the assimilation of the SWIR TROPOMI TCCO retrievals provides additional information to the CAMS system that is already constrained by the TIR MOPITT and IASI TCCO data in CTRL. At the West African airports, the improvement is largest above 800 hPa. Here, the number of clear data is lower than in the other areas, reducing the sensitivity of TROPOMI to near surface CO.

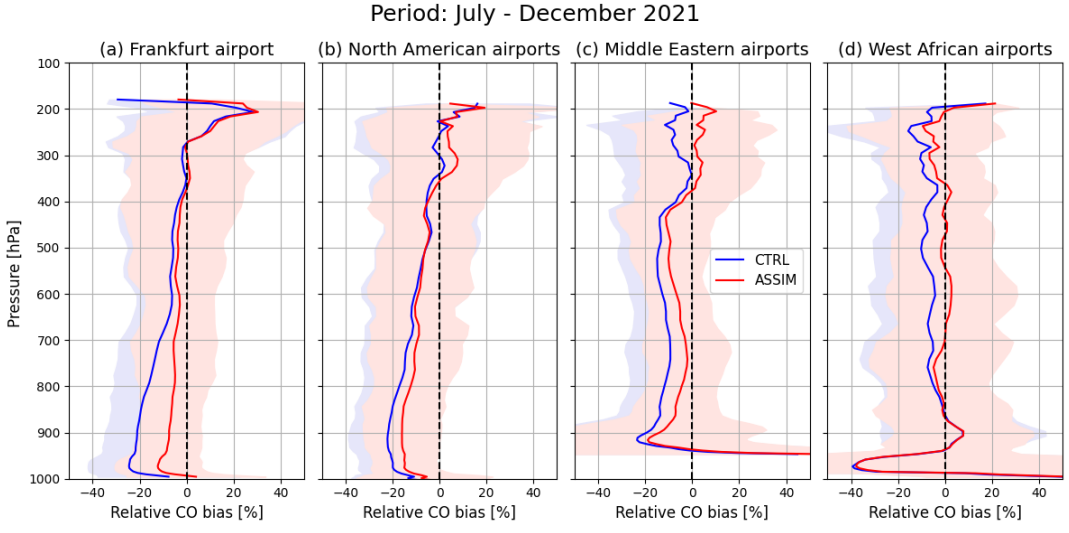

Figure 16: Relative difference in % of CO profiles from ASSIM (red) and CTRL (blue) against IASI aircraft data at (a) Frankfurt airport and averaged over (b) North American, (c) Middle Eastern and (d) West African airports averaged over the period July to December 2021. The shaded areas denote ± 1 standard deviation.

https://doi.org/10.5194/acp-2022-458
Preprint. Discussion started: 4 July 2022

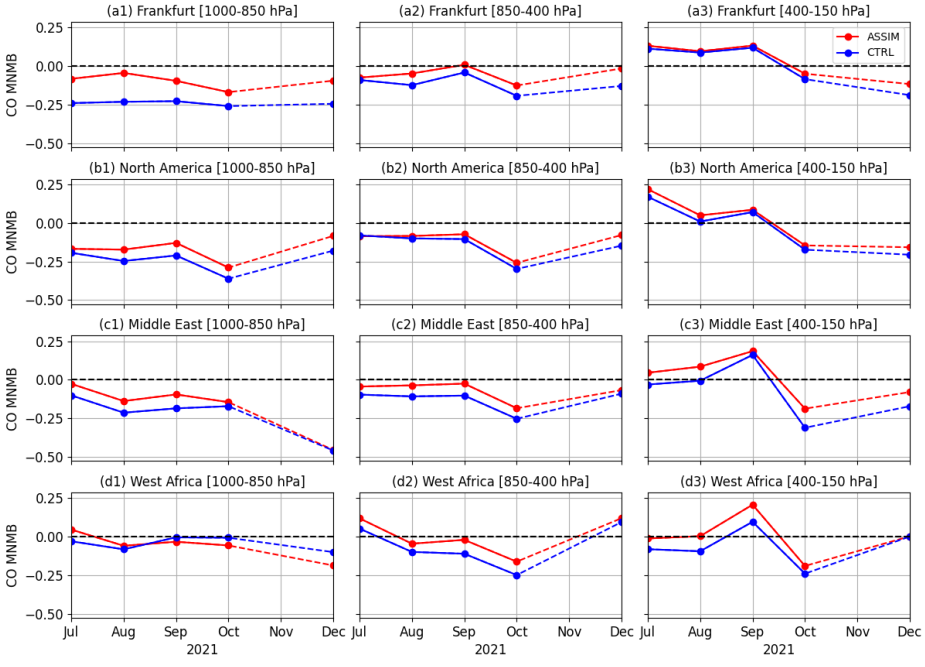

Figure 17: Time series of monthly mean modified normalised mean bias (MNMB) against IAGOS data for the period July to December 2021 at (a) Frankfurt airport, (b) North American, (c) Middle Eastern and (d) West African airports for the layers (1) 1000-850 hPa, (2) 850-400 hPa and (3) 400-150 hPa.

The final comparison is against CO surface air quality observations from the European Airbase network, the US Airnow network and Chinese air quality data (Fig. 18). We find an improved fit to the surface observations and a reduction of the negative MNMB in ASSIM over Europe and North America as the assimilation of TROPOMI CO data leads to changes in surface ozone. There is a much smaller impact over China.

https://doi.org/10.5194/acp-2022-458
Preprint. Discussion started: 4 July 2022

Atmospheric Chemistry and Physics Discussions

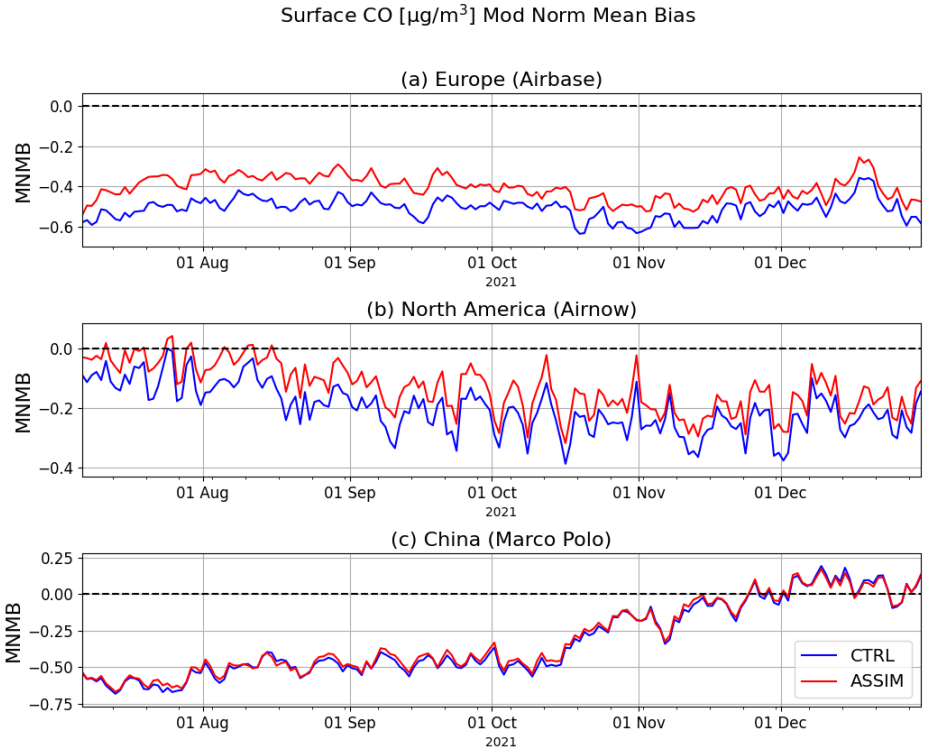

Figure 18: Timeseries of MNMB of surface CO values from ASSIM (red) and CTRL (blue) from (a) European Airbase stations, (b) North American Airnow stations and (c) Chinese air quality data. AirBase (http://acm.eionet.europa.eu/databases/airbase/) is the public air quality database system of the European Environmental Agency (EEA; http://www.eea.europa.eu/). Airnow (www.airnow.gov) reports air quality for the US. More than 1,500 in situ stations covering all major cities in China are operated by the China National Environmental Monitoring Center, providing hourly observations of several pollutants, including CO (Bai et al., 2020). Data can be accessed via websites of third parties (such as http://www.pm25.in and http://www.aqicn.org).

The comparisons against independent CO observations in this section show that the assimilation of NRT TROPOMI CO data in the CAMS global system reduces the negative bias of the CAMS CO analysis in the troposphere and has the largest impact in the lower and free troposphere. This is because the SWIR TROPOMI CO retrieval is sensitive to the CO column, including contributions from the boundary layer, especially for clear data. It therefore provides additional information for the CAMS CO analysis which is already constrained by the assimilation of TIR MOPITT and IASI CO retrievals that are most sensitive to CO in the mid-troposphere.

4.2.4 Boreal wildfires July and August 2021

High temperatures and drought conditions increase the risk of wildfires and led to the development of strong and persistent wildfires between June and August 2021 across many parts of North America, particularly in the western United States and Canada, with the so-called ‘Dixie fire’ in northern California one of the biggest ever recorded in the state's history. Boreal wildfire activity in 2021 was also strong in Siberia, particularly in the Sakha Republic of Russia, over the same period. The Global Fire Assimilation System (GFAS; Kaiser et al., 2012) run by CAMS to produce daily information of fire activity, showed persistent high daily intensity of the fires in Canada, the US and Siberia in July and August 2021 (Fig. 19), with record annual total biomass burning CO emissions for 2021 of 46 Tg (Siberia), 17 Tg (Canada) and 9 Tg (US).

https://doi.org/10.5194/acp-2022-458
Preprint. Discussion started: 4 July 2022

Atmospheric Chemistry and Physics Discussions

The CAMS global NRT forecasts captured the transport of smoke from the persistent large-scale Siberian and North American wildfires. In July and August 2021, thick smoke from the North American wildfires was transported eastwards across North America in several episodes. It was observed at many Aeronet sites (not shown) and led at times to severely degraded air quality as far away as the north-eastern US coast, with haze clearly apparent in New York City. Satellite images, Aeronet observations and CAMS forecasts showed that smoke from some of the North American fires was transported further across the North Atlantic Ocean, passing Greenland, and reaching Europe. A concern with such high amounts of smoke crossing Greenland is the potential deposition of black carbon to the ice sheet, and previous studies have shown smoke particles from Canadian wildfires in the snowpack (Thomas et al., 2017). A very high number of wildfires also burned in eastern Russia through July and early August with the worst affected area the Sakha Republic. In terms of the total estimated wildfire carbon emissions for June-August in the Sakha Republic, a new record in the GFAS period was set in early August 2021, when the cumulative daily total emissions for 2021 were already larger than annual total of the previous record year 2020. CO from these fires was transported north across the Arctic Ocean as far as the North Pole. Figure 20 shows maps of daily TCCO from ASSIM from 4 to 23 August 2021, depicting CO from the strong fires in Eastern Russia, the North American fires, and several of the episodes of CO transport from North America eastwards over the Atlantic and from Siberia over the North Pole. Note that on 6 August 2021 some of the highest CO columns globally were found over the normally clean North Pole.

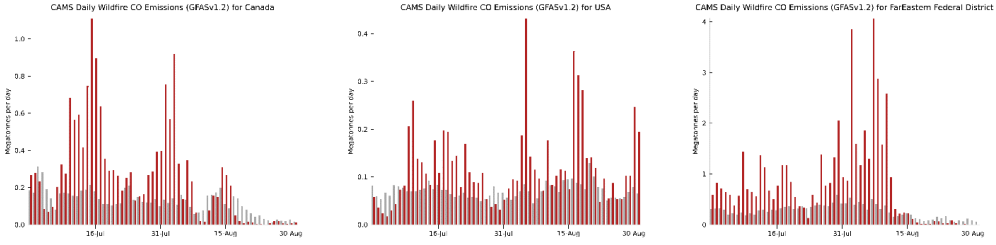

Figure 19: GFAS v1.2 daily total CO emissions in Mt/day for Canada (left), the USA (middle) and Eastern Russia (right) in July and August 2021 (red bars show 2021, grey bars show 2003-2020 mean).

https://doi.org/10.5194/acp-2022-458
Preprint. Discussion started: 4 July 2022

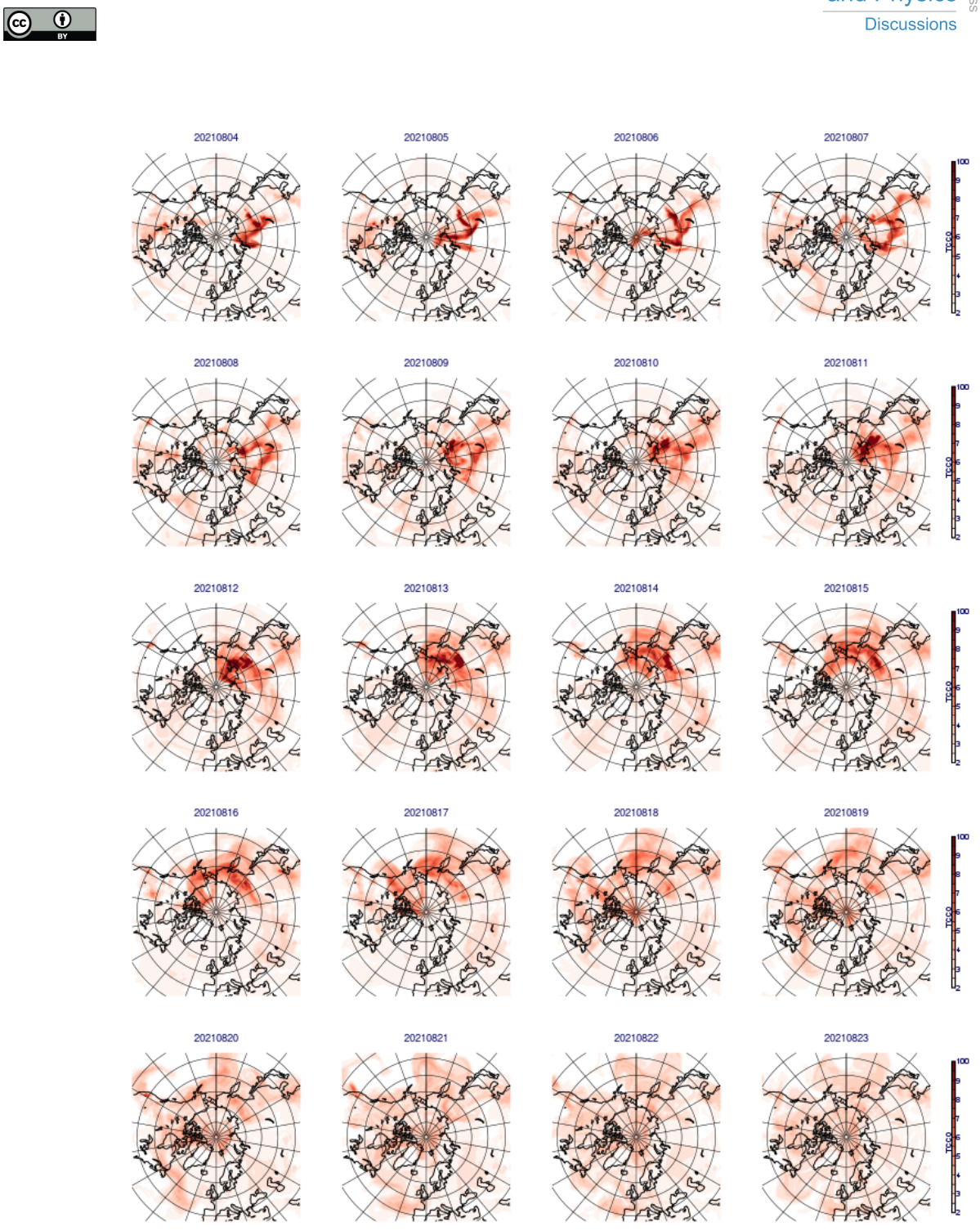

Figure 20: TCCO fields in 10^{18} molec/cm^2 from ASSIM for the period 4 to 23 August 2021.

The August 2021 average TCCO field from TROPOMI and IASI-C showed the highest CO columns over Siberia as well as elevated values over North America, the North Pacific, North Atlantic and Arctic Ocean (Fig. 21). The same was seen for IASI-B (not shown). These high values are better captured in ASSIM than in CTRL, as seen by the smaller IASI-C analysis

https://doi.org/10.5194/acp-2022-458
Preprint. Discussion started: 4 July 2022

Atmospheric Chemistry and Physics Discussions

departures in ASSIM, in the area north of 65°N where IASI data are not assimilated. This better agreement was already shown in Section 4.2.2 in the timeseries of departures averaged over the Arctic latitudes (Fig. 13).

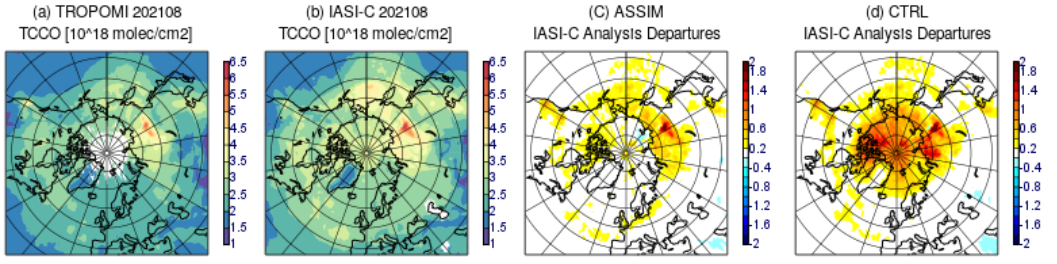

Figure 21: August 2021 monthly mean (a) TROPOMI TCCO field, (b) IASI-C TCCO field, (c) IASI-C analysis departures from ASSIM and (d) IASI-C analysis departures from CTRL in 10^{18} molec/cm^2.

Some IAGOS flights in August 2021 intersected parts of the CO plumes that were transported eastwards over North America and further over the Atlantic. Figure 22 shows CO profiles at Boston and New York airports on 6 August which crossed such a plume, visible in the CO values greater than 150 ppb above 500 hPa. The subsequent profile at New York (Fig. 22c) on 7 August still showed the remnants of the plume with values greater than 100 ppb between 450 and 350 hPa. Both ASSIM and CTRL have elevated CO values above 500 hPa at both airports on 6 August, but do not quite reach the values seen in the observations. The vertical structure of the CO profile is reproduced better in ASSIM than in CTRL, but the largest improvement is found in the lower troposphere in all 3 cases, and the actual impact at the plume altitude is smaller.

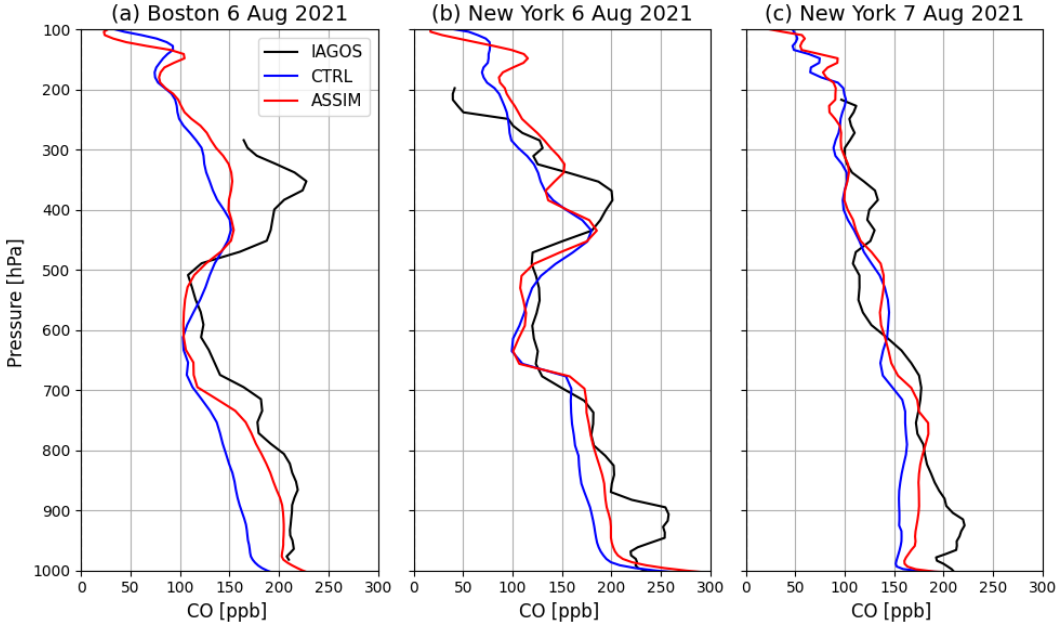

Figure 22: CO profiles in ppb from IAGOS (black), ASSIM (red) and CTRL (blue) at (a) Boston on 6 August, (b) New York on 6 August and (c) New York on 7 August 2021 in ppb.

Figure 23 shows CO profiles at Frankfurt airport when plumes of smoke from the North American wildfires reached Europe on 7, 9 and 11 August 2021. These plumes led to elevated CO values above 500 hPa on 7 and 9 August, with maximum values located around 400 hPa and exceeding 300 ppb and 250 ppb, respectively. On 11 August the plume was located at lower

https://doi.org/10.5194/acp-2022-458
Preprint. Discussion started: 4 July 2022

Atmospheric Chemistry and Physics Discussions

altitude (between 600 and 500 hPa) and only had values of about 180 ppb. ASSIM and CTRL show elevated CO values above 500 hPa on 7 August, but maximum CO values remain below 200 ppb. On 9 August, the plume is located at higher altitude in ASSIM and CTRL than in the observations. The weaker plume on 11 August is captured to some extent in ASSIM but does again not reach the values seen in the observations. As at the North American airports (Fig. 22) the largest improvement in ASSIM compared to CTRL is found in the lower and free troposphere, i.e., below the altitude of the plumes. The final example is given in Fig. 24 when elevated CO values are again observed over Frankfurt airport between 19-21 August 2021. ASSIM and CTRL both show elevated CO values in the upper troposphere, with larger values in ASSIM on 19 and 21 August, but the maximum values of about 180 ppb seen in the observations above 300 hPa are not quite reached. On 20 August both ASSIM and CTRL still show the plume, while the observations do not show it anymore. This might be because of a horizontal mismatch of the plume location in model and observations. Figure 24 again illustrates that the largest improvement from the assimilation of TROPOMI CO data in ASSIM is found in the lower and mid-troposphere. In the upper troposphere the CAMS analysis is already constrained by the assimilated TIR MOPITT and IASI data, and the additional impact from the TROPOMI data is smaller.

Considering that only total column CO data are assimilated in the CAMS system, the improvements in the CO profiles in ASSIM seen in Fig. 22-24 can be considered a success. Figure 25 depicts weekly average CO profiles at Frankfurt airport between 26 July and 29 August 2021 and shows clearly the improved fit to the IAGOS profiles below about 500 hPa in ASSIM. Figure 25 also shows that the high CO values seen in IAGOS profiles between 500-400 hPa in the week 2-8 August are not quite captured in either model run.

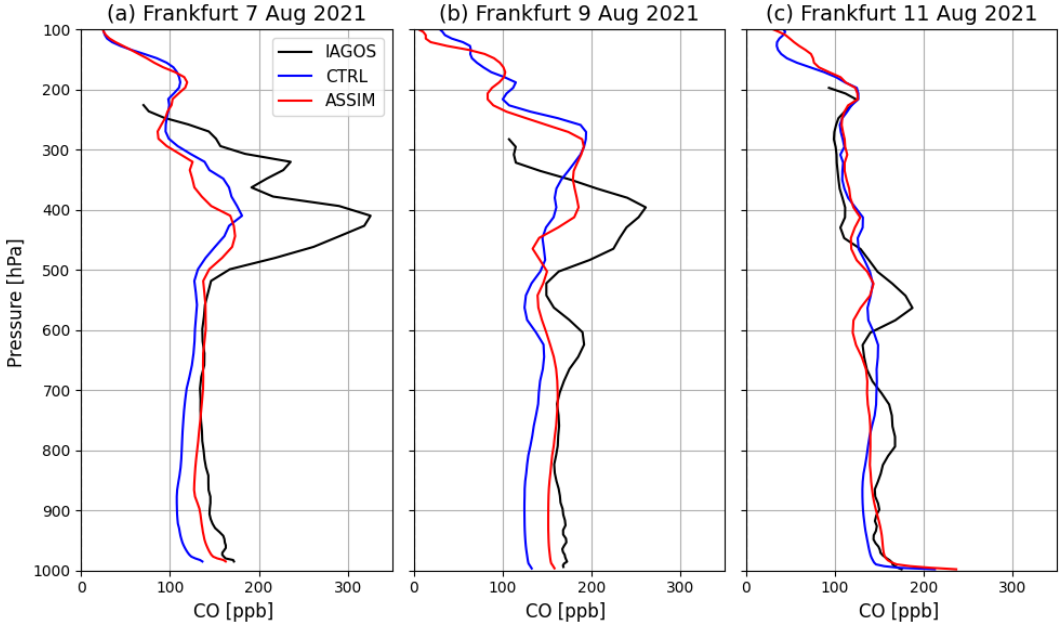

Figure 23: Like Fig. 22 but at Frankfurt on (a) 7 August, (b) 9 August and (c) 11 August 2021.

https://doi.org/10.5194/acp-2022-458
Preprint. Discussion started: 4 July 2022

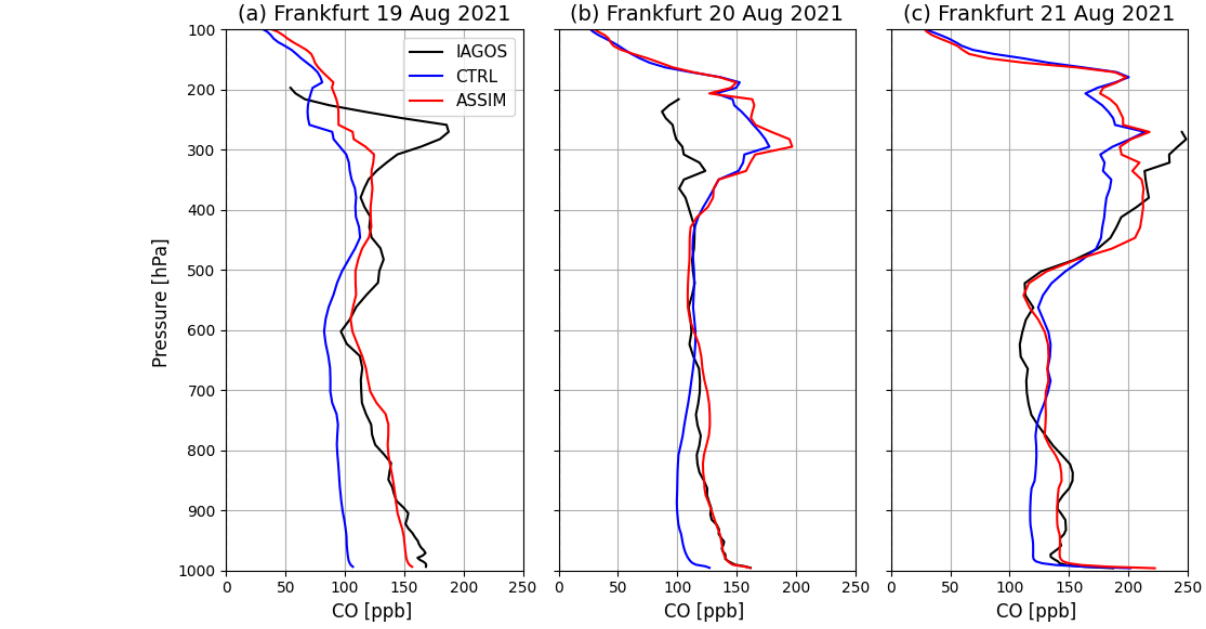

Figure 24: Like Fig. 22 but at Frankfurt on (a) 19 August, (b) 20 August and (c) 21 August 2021.

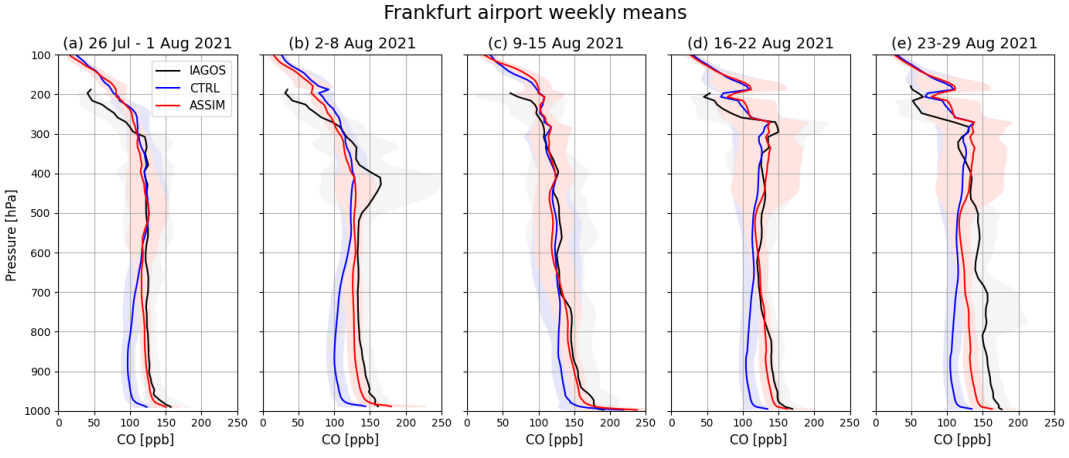

Figure 25: Weekly mean CO profiles in ppb from IAGOS (black), ASSIM (red) and CTRL (blue) at Frankfurt for the weeks commencing (a) 26 July, (b) 2 August, (c) 9 August, (d) 16 August and (e) 23 August 2021.

5 Conclusions

Operational near-real time TROPOMI total column CO data have been monitored passively in the CAMS global data assimilation system, which assimilates IASI and MOPITT TIR TCCO data, since November 2018. The TROPOMI data successfully capture the global TCCO distribution with high values in the NH, lower values in the SH, high values in areas of anthropogenic pollution in SE Asia, North America and Europe, as well as in the biomass burning areas in the Tropics and boreal fire regions. In the global mean, CAMS TCCO analysis values are about 10% lower than TROPOMI TCCO (averaged over the period November 2018 to Dec 2021), with the smallest relative differences found for clear-sky data in the Tropics

https://doi.org/10.5194/acp-2022-458
Preprint. Discussion started: 4 July 2022


Atmospheric Chemistry and Physics Discussions

(6.6 %) and the largest relative differences (11-14%) found in the polar latitude bands, i.e., the areas where no satellite CO retrievals are assimilated in the global CAMS system.

Timeseries of TROPOMI observation values and analysis departures show differences between clear and cloudy TROPOMI TCCO data over land, as well as differences between cloudy data over land and oceans, both in terms of seasonality of the observations as well as seasonality and magnitude of TROPOMI analysis departures. The reason for this is not fully understood yet. These timeseries also capture the impact of upgrades to the CAMS model or the TROPOMI retrieval algorithm, with the largest change resulting from the CAMS model upgrade to CY46R1 in July 2019. This upgrade included a change of emission inventories and led to an increased negative CO bias of the CAMS model and hence increased positive TROPOMI departures (from departures of 5-10% to 10-15% when averaged over all 'good' TROPOMI data globally). Reduced departures are seen after the TROPOMI algorithm update to version 02.02.00 in early July 2021 and the CAMS model upgrade to CY47R3 in October 2021, after which the departures averaged globally for all good TROPOMI TCCO data were around 8%.

The monitoring timeseries show pronounced differences between clear and cloudy TROPOMI data over land. The TROPOMI SWIR CO retrieval under clear-sky atmospheric condition shows a good sensitivity throughout the atmosphere, including contributions from near surface CO. Retrievals from cloudy measurements exhibit a reduced sensitivity in the lower troposphere caused by shielding of the clouds in the observation geometry of the satellite. Therefore, the retrieved TROPOMI TCCO values have contributions from different parts of the CO profile to the total column for clear and cloudy data, and it is important to take the TROPOMI averaging kernels into account when comparing CAMS and TROPOMI data. By doing this, the CAMS CO column smoothed by the TROPOMI total averaging kernels can be compared with the TROPOMI TCCO values in a like-with-like manner. The CAMS system applies the TROPOMI averaging kernels in the observation operator when assimilating the data. Single observation experiments show that the assimilation of clear-sky TROPOMI data has a larger impact in the lower troposphere and at the surface, while cloudy data have a larger impact on changing the CAMS field in the free and upper troposphere, because of the different vertical sensitivities of the clear-sky and cloudy observations as given by their averaging kernels.

The assimilation of TROPOMI CO improves the fit to the also assimilated IASI-BC TCCO data but degrades the fit to MOPITT TCCO. The NRT MOPITT CO columns have lower values than IASI and TROPOMI data, and by adding TROPOMI to the assimilation system the impact of the MOPITT data is reduced and the analysis draws less strongly to those data. When TROPOMI data are assimilated in the CAMS system, they lead to increased CO analysis values and an improved fit to independent observations. The impact of the TROPOMI assimilation is large, with TCCO changes of over 50% in the CAMS analysis at high northern latitudes during July and August 2021 when unusually strong boreal wildfires led to unprecedented amounts of CO being released into the atmosphere. The TROPOMI CO assimilation also has a large impact on the vertical distribution of CO in the CAMS analysis and leads to increased CO analysis values at the surface and in the troposphere in the NH, and in the upper troposphere in the Tropics. It improves the fit to IAGOS aircraft data, with the largest absolute and relative CO increase found in the lower and the free troposphere, where the global CAMS NRT system is known to have a negative bias. Here, the assimilation of TROPOMI CO data improves the fit to IAGOS aircraft profiles in Europe (Frankfurt airport), at North American, West African, and Middle Eastern airports. Furthermore, comparison with NDACC FTIR data tropospheric and total column CO data, and with surface air quality CO data in North America (AirNow), Europe (AirBase) and China (Marco Polo) also show reduced negative biases when TROPOMI CO data are assimilated.

TROPOMI monitoring timeseries also show increased CO columns due to boreal wildfires during NH summers and due to the 2019/2020 Australian bushfires in the SH. In particular, the NH summer of 2021 saw strong wildfires in North America and

https://doi.org/10.5194/acp-2022-458
Preprint. Discussion started: 4 July 2022

Russia that released record amounts of CO into the atmosphere (46 Tg in Siberia, 17 Tg in Canada and 9 Tg in the US according to GFAS v1.2 data). Plumes of smoke from the Siberian fires were transported to polar latitudes, leading to some of the highest CO columns globally on 6 August at the normally clean North Pole, and from North America eastwards over the North Atlantic, reaching as far as Europe. These transport events were clearly visible in the CAMS CO analysis fields. The assimilation of TROPOMI CO improved the fit to IASI CO data in the Arctic during the period of intense burning in July and August 2021, by increasing the CAMS TCCO analysis values. Some of the plumes of high CO in the upper troposphere were intersected by IAGOS aircraft at Boston, New York, and Frankfurt airport. These plumes were also captured in the CAMS CO analysis, but the magnitude of the upper-level CO maxima was usually lower than in the observations. At these altitudes, the assimilation of TROPOMI did not change the CAMS CO field much, compared to a model run that already assimilated MOPITT and IASI TCCO.

The results of this paper illustrate that the use of TROPOMI TCCO data in the global CAMS system is beneficial, and consequently the TROPOMI CO assimilation will be activated in the next operational upgrade (CY48R1) of the CAMS global system which is scheduled for Q1/2023. The TROPOMI CO data, retrieved from the SWIR part of the solar spectrum, are sensitive to CO throughout the troposphere, including contributions from the surface, while the TCCO data that are already assimilated by CAMS (i.e. TIR MOPITT and IASI TCCO) have the largest sensitivity in the mid-troposphere. TROPOMI therefore brings additional information on the vertical CO distribution into the CAMS analysis in parts of the column where CO is not already well constrained by the assimilation of TIR MOPITT and IASI TCCO retrievals. The largest contribution from near-surface CO is found for clear-sky TROPOMI CO retrievals, while the impact in the lower troposphere is reduced for cloudy scenes.

Author Contributions

A. Inness carried out the experiments described in the paper, the validation of the resulting analysis fields and wrote the manuscript. R. Ribas set up the S5P processing chain at ECMWF which included coding and testing the BUFR converter needed to ingest the TROPOMI TCCO data in the ECMWF data system. J. Flemming helped with the development of the IFS chemistry module. M. Parrington contributed to the section on wildfires and produced Fig. 19. M. Ades worked on the development of the CAMS background errors. B. Langerock carried out the validation with NDACC FTIR data and produced Fig. 3, 14, 15. T. Borsdorff and J. Landgraf developed the TROPOMI TCCO retrieval, and I. Aben is the TROPOMI co-Principal Investigator. All co-authors gave useful comments during the writing of the paper.

Acknowledgements

The Copernicus Atmosphere Monitoring Service is operated by the European Centre for Medium-Range Weather Forecasts on behalf of the European Commission as part of the Copernicus programme (http://copernicus.eu). T. Borsdorff acknowledges funding from the TROPOMI national programme through NSO. Thanks to Sebastien Massart for his pywave tool that helped to analyse the background error matrices, Luke Jones for the profile_browse and ver0D tools to validate against IAGOS and surface CO observations, and Mohamed Dahoui for help with obstat. The NDACC FTIR data used in this publication were obtained from NDACC PIs (Arrival Heights; NIWA; Smale; Daniel; Boulder; NCAR; Hannigan; James; Garmisch; KIT/IMK-IFU; Sussmann; RalfIzana; KIT; Schneider; Matthias; Jungfraujoch; ULG; Mahieu; Emmanuel; Kiruna; KIT; Blumenstock; Thomas; La Reunion ; BIRA.IASB; De Mazière; Martine; Lauder; NIWA; Smale; Daniel; Mauna Loa; NCAR; Hannigan; James; St. Petersburg; SPBU; Makarova ; Maria; Thule; NCAR; Hannigan; James, W.; Toronto; UTORONTO; Strong; Kimberly; Wollongong; UOW; Jones; Nicholas; Zugspitze; KIT/IMK-IFU; Sussmann; Ralf) as part of the Network for the

https://doi.org/10.5194/acp-2022-458
Preprint. Discussion started: 4 July 2022

Detection of Atmospheric Composition Change (NDACC) and are available through the NDACC website www.ndacc.org. The National Center for Atmospheric Research is sponsored by the National Science Foundation. The NCAR FTS observation programs at Thule, GR, Boulder, CO and Mauna Loa, HI are supported under contract by the National Aeronautics and Space Administration (NASA). We wish to thank the Danish Meteorological Institute for support at the Thule site and NOAA for support of the MLO site. The NDACC FTIR stations (Bremen, Garmisch, Izaña, Ny-Ålesund) have been supported by the German Bundesministerium für Wirtschaft und Energie (BMWi) via DLR under grants 50EE1711A, B and D. The multi-decadal FTIR monitoring program of ULiège at the Jungfraujoch station has been primarily supported by the F.R.S.-FNRS (Brussels, Belgium) and by the GAW-CH programme of MeteoSwiss. The International Foundation High Altitude Research Stations Jungfraujoch and Gornergrat (HFSJG, Bern) supported the facilities needed to perform the FTIR observations.

The output from the two experiments used in this study is available from https://apps.ecmwf.int/research-experiments/expver/ (last access 26/10/2021) using the following DOIs:

- hmib (Inness, 2022a): https://doi.org/10.21957/ax0c-fm72
- hlxm (Inness, 2022b): https://doi.org/10.21957/mwqe-vs95

References

Bai, K., Li, K., Guo, J., Yang, Y., & Chang, N.-B.: Filling the gaps of in situ hourly PM2.5 concentration data with the aid of empirical orthogonal function analysis constrained by diurnal cycles, Atmospheric Measurement Techniques, 13(3), 1213–1226, https://doi.org/10.5194/amt-13-1213-2020, 2020.

Benedetti, A., Morcrette, J.-J., Boucher, O., Dethof, A., Engelen, R. J., Fisher, M., Flentje, H., Huneeus, N., Jones, L., Kaiser, J. W., Kinne, S., Mangold, A., Razinger, M., Simmons, A. J., Suttie, M., and the GEMS-AER team: Aerosol analysis and forecast in the European Centre for Medium-Range Weather Forecasts Integrated Forecast System: Data Assimilation. J. Geophys. Res., D13205, 114, doi:10.1020/2008JD011115, 2009.

Borsdorff, T., Aan de Brugh, J., Hu, H., Aben, I., Hasekamp, O., & Landgraf, J.: Measuring carbon monoxide with TROPOMI: First results and a comparison with ECMWF-IFS analysis data, Geophysical Research Letters, 45, 2826–2832, https://doi.org/10.1002/2018GL077045, 2018.

Borsdorff, T., Hasekamp, O. P., Wassmann, A., and Landgraf, J.: Insights into Tikhonov regularization: application to trace gas column retrieval and the efficient calculation of total column averaging kernels, Atmos. Meas. Tech., 7, 523–535, https://doi.org/10.5194/amt-7-523-2014, 2014.

Clerbaux, C., Boynard, A., Clarisse, L., George, M., Hadji-Lazaro, J., Herbin, H., Hurtmans, D., Pommier, M., Razavi, A., Turquety, S., Wespes, C., and Coheur, P.-F.: Monitoring of atmospheric composition using the thermal infrared IASI/MetOp sounder, Atmos. Chem. Phys., 9, 6041-6054, 2009.

Courtier, P., Thépaut, J.-N. and Hollingsworth, A.: A strategy for operational implementation of 4D-Var, using an incremental approach, Q. J. R. Meteorol. Soc., 120, 1367-1388, 1994.

Dee, D. P. and Uppala, S.: Variational bias correction of satellite radiance data in the ERA-Interim reanalysis, Q. J. R. Meteorol. Soc, 135, 1830–1841, 2009.

https://doi.org/10.5194/acp-2022-458
Preprint. Discussion started: 4 July 2022

Deeter, M. N., Edwards, D. P., Francis, G. L., Gille, J. C., Martínez-Alonso, S., Worden, H. M., and Sweeney, C.: A climate-scale satellite record for carbon monoxide: the MOPITT Version 7 product, Atmos. Meas. Tech., 10, 2533-2555, https://doi.org/10.5194/amt-10-2533-2017, 2017.

Deeter, M. N., Edwards, D. P., Francis, G. L., Gille, J. C., Mao, D., Martínez-Alonso, S., Worden, H. M., Ziskin, D., and Andreae, M. O.: Radiance-based retrieval bias mitigation for the MOPITT instrument: the version 8 product, Atmos. Meas. Tech., 12, 4561–4580, https://doi.org/10.5194/amt-12-4561-2019, 2019.

Deeter, M., Francis, G., Gille, J., Mao, D., Martínez-Alonso, S., Worden, H., Ziskin, D., Drummond, J., Commane, R., Diskin, G., and McKain, K.: The MOPITT Version 9 CO Product: Sampling Enhancements and Validation, Atmos. Meas. Tech. Discuss. [preprint], https://doi.org/10.5194/amt-2021-370, in review, 2021.

Deeter, M. N., Martínez-Alonso, S., Edwards, D. P., Emmons, L. K., Gille, J. C. , Worden, H. M., Pittman, J. V., Daube, B. C. and Wofsy, S. C.: Validation of MOPITT Version 5 thermal-infrared, near-infrared, and multispectral carbon monoxide profile retrievals for 2000–2011, J. Geophys. Res. Atmos., 118, 6710–6725, doi:10.1002/jgrd.50272, 2013.

Errera, Q., M. Ramonet, N. Sudarchikova, M. Schulz. H. J. Eskes, S. Basart, A. Benedictow, Y. Bennouna, A.-M. Blechschmidt, S. Chabrillat, Christophe, Y., E. Cuevas, A. El-Yazidi, H. Flentje, P. Fritzsche, K.M. Hansen, U. Im, J. Kapsomenakis, B. Langerock, A. Richter, V. Thouret, A. Wagner, T. Warneke, C. Zerefos, Validation report of the CAMS near-real-time global atmospheric composition service: Period March – May 2021, Copernicus Atmosphere Monitoring Service (CAMS) report, CAMS84_2018SC3_D1.1.1_MAM2021.pdf, September 2021, doi:10.24380/qq5m- dg18, 2021.

Fisher, M.: Generalized frames on the sphere with application to background error covariance modelling. Seminar on recent developments in numerical methods for atmospheric and ocean modelling, 6-10 September 2004, Proceedings, ECMWF, https://www.ecmwf.int/node/9405 (last access: 30 June 2022), 2004.

Fisher, M. and Andersson, E.: Developments in 4D-Var and Kalman Filtering, ECMWF Technical Memorandum 347, ECMWF, Shinfield Park, Reading, 10.21957/5ghofnp6c, 2001.

Flemming, J. and A. Inness: Carbon Monoxide [in "State of the Climate in 2020"], Bull. Amer. Meteor., 102 (8), S101–S102, https://doi.org/10.1175/BAMS-D-21-0098.1, 2021.

Flemming, J., Benedetti, A., Inness, A., Engelen, R. J., Jones, L., Huijnen, V., Remy, S., Parrington, M., Suttie, M., Bozzo, A., Peuch, V.-H., Akritidis, D., and Katragkou, E.: The CAMS interim Reanalysis of Carbon Monoxide, Ozone and Aerosol for 2003–2015, Atmos. Chem. Phys., 17, 1945-1983, https://doi.org/10.5194/acp-17-1945-2017, 2017.

Flemming, J., Huijnen, V., Arteta, J., Bechtold, P., Beljaars, A., Blechschmidt, A.-M., Diamantakis, M., Engelen, R. J., Gaudel, A., Inness, A., Jones, L., Josse, B., Katragkou, E., Marecal, V., Peuch, V.-H., Richter, A., Schultz, M. G., Stein, O., and

https://doi.org/10.5194/acp-2022-458
Preprint. Discussion started: 4 July 2022

Tsikerdekis, A.: Tropospheric chemistry in the Integrated Forecasting System of ECMWF, Geosci. Model Dev., 8, 975-1003, doi:10.5194/gmd-8-975-2015, 2015.

Fortems-Cheiney, A., Chevallier, F., Pison, I., Bousquet, P., Szopa, S., Deeter, M. N., and Clerbaux, C.: Ten years of CO emissions as seen from Measurements of Pollution in the Troposphere (MOPITT), J. Geophys. Res., 116, D05304, doi:10.1029/2010JD014416, 2011.

Garrigues, S., Remy, S., Chimot, J., Ades, M., Inness, A., Flemming, J., Kipling, Z., laszlo, I., Benedetti, A., Ribas, R., Jafariserajehlou, S., Fougnie, B., Kondragunta, S., Engelen, R., Peuch, V.-H., Parrington, M., Bousserez, N., Vazquez Navarro, M., and Agusti-Panareda, A.: Monitoring multiple satellite Aerosol Optical Depth (AOD) products within the Copernicus Atmosphere Monitoring Service (CAMS) data assimilation system, Atmos. Chem. Phys. Discuss. [preprint], https://doi.org/10.5194/acp-2022-176, in review, 2022.

Gaubert, B., Arellano Jr., A. F., Barré, J., Worden, H. M., Emmons, L. K., Tilmes, S., Buchholz, R. R., Vitt, F., Raeder, K., Collins, N., Anderson, J. L., Wiedinmyer, C., Martinez Alonso, S., Edwards, D. P., Andreae, M. O., Hannigan, J. W., Petri, C., Strong, K. and Jones, N.: Toward a chemical reanalysis in a coupled chemistry-climate model: An evaluation of MOPITT CO assimilation and its impact on tropospheric composition, J. Geophys. Res. Atmos., 121, 7310– 7343, doi:10.1002/2016JD024863, 2016.

George, M., Clerbaux, C., Hurtmans, D., Turquety, S., Coheur, P.-F., Pommier, M., Hadji-Lazaro, J., Edwards, D. P., Worden, H., Luo, M., Rinsland, C., and McMillan, W.: Carbon monoxide distributions from the IASI/METOP mission: evaluation with other space-borne remote sensors, Atmos. Chem. Phys., 9, 8317–8330, 2009.

George, M., Clerbaux, C., Bouarar, I., Coheur, P.-F., Deeter, M. N., Edwards, D. P., Francis, G., Gille, J. C., Hadji-Lazaro, J., Hurtmans, D., Inness, A., Mao, D., and Worden, H. M.: An examination of the long-term CO records from MOPITT and IASI: comparison of retrieval methodology, Atmos. Meas. Tech., 8, 4313-4328, https://doi.org/10.5194/amt-8-4313-2015, 2015.

Granier, C., Bessagnet, B., Bond, T., D'Angiola, A., Denier van der Gon, H., Frost, G. J., Heil, A., Kaiser, J. W., Kinne, S., Klimont, Z., Kloster,S., Lamarque, J.-F., Liousse, C., Masui, T., Meleux, F., Mieville, A., Ohara, R., Raut, J.-C., Riahi, K., Schultz, M. G., Smith, S. G., Thompson, A., van Aardenne, J., van der Werf, G. R., and van Vuuren, D. P.: Evolution of anthropogenic and biomass burning emissions of air pollutants at global and regional scales during the 1980-2010 period, Climatic Change, 109, 163-190. DOI: 10.1007/s 10584-011-0154-1, 2011.

Granier, C., Darras, S., , Denier van der Gon, H., Doubalova, J., Elguindi, N., Galle, B., Gauss, M., Guevara, M., Jalkanen, J.-P., Kuenen, J., Liousse, C., Quack, B., Simpson, D., and Sindelarova, K.: The Copernicus Atmosphere Monitoring Service global and regional emissions (April 2019 version), Copernicus Atmosphere Monitoring Service (CAMS) report, doi:10.24380/d0bn-kx16, 2019.

Griffin RJ, Chen JJ, Carmody K, Vutukuru S, Dabdub D.: Contribution of gas phase oxidation of volatile organic compounds to atmospheric carbon monoxide levels in two areas of the United States, Journal of Geophysical Research-Atmospheres 112: D10S17. doi:10.1029/2006JD007602, 2007.

https://doi.org/10.5194/acp-2022-458
Preprint. Discussion started: 4 July 2022

Guenther, A., Karl, T., Harley, P., Wiedinmyer, C., Palmer, P. I., and Geron, C.: Estimates of global terrestrial isoprene emissions using MEGAN (Model of Emissions of Gases and Aerosols from Nature), Atmos. Chem. Phys., 6, 3181–3210, doi:10.5194/acp-6- 3181-2006, 2006.

Hase, F., T. Blumenstock, S. Dohe, J. Groß, M. Kiel.: TCCON data from Karlsruhe, Germany, Release GGG2014R0. TCCON data archive, hosted by the Carbon Dioxide Information Analysis Center, Oak Ridge National Laboratory, Oak Ridge, Tennessee, U.S.A. http://dx.doi.org/10.14291/tccon.ggg...e01.R0/1149270, 2014.

Hudman, R. C., Murray, L. T., Jacob, D. J., Millet, D. B., Turquety, S., Wu, S., Blake, D. R., Goldstein, A. H., Holloway, J., Sachse, G. W.: Biogenic versus anthropogenic sources of CO over the United States, Geophysical Research Letters 35, L04801, 2008.

Huijnen, V., Pozzer, A., Arteta, J., Brasseur, G., Bouarar, I., Chabrillat, S., Christophe, Y., Doumbia, T., Flemming, J., Guth, J., Josse, B., Karydis, V. A., Marécal, V., and Pelletier, S.: Quantifying uncertainties due to chemistry modelling – evaluation of tropospheric composition simulations in the CAMS model (cycle 43R1), Geosci. Model Dev., 12, 1725–1752, https://doi.org/10.5194/gmd-12-1725-2019, 2019

Huijnen, V., Williams, J., van Weele, M., van Noije, T., Krol, M., Dentener, F., Segers, A., Houweling, S., Peters, W., de Laat, J., Boersma, F., Bergamaschi, P., van Velthoven, P., Le Sager, P., Eskes, H., Alkemade, F., Scheele, R., Nédélec, P., and Pätz, H.-W.: The global chemistry transport model TM5: description and evaluation of the tropospheric chemistry version 3.0, Geosci. Model Dev., 3, 445-473, doi:10.5194/gmd-3-445-2010, 2010.

Inness, A., Baier, F., Benedetti, A., Bouarar, I., Chabrillat, S., Clark, H., Clerbaux, C., Coheur, P., Engelen, R. J., Errera, Q., Flemming, J., George, M., Granier, C., Hadji-Lazaro, J., Huijnen, V., Hurtmans, D., Jones, L., Kaiser, J. W., Kapsomenakis, J., Lefever, K., Leitão, J., Razinger, M., Richter, A., Schultz, M. G., Simmons, A. J., Suttie, M., Stein, O., Thépaut, J.-N., Thouret, V., Vrekoussis, M., Zerefos, C., and the MACC team: The MACC reanalysis: an 8 yr data set of atmospheric composition, Atmos. Chem. Phys., 13, 4073–4109, https://doi.org/10.5194/acp-13-4073-2013, 2013.

Inness, A., Benedetti, A., Flemming, J., Huijnen, V., Kaiser, J. W., Parrington, M., and Remy, S.: The ENSO signal in atmospheric composition fields: emission-driven versus dynamically induced changes, Atmos. Chem. Phys., 15, 9083–9097, https://doi.org/10.5194/acp-15-9083-2015, 2015b.

Inness, A., Blechschmidt, A.-M., Bouarar, I., Chabrillat, S., Crepulja, M., Engelen, R. J., Eskes, H., Flemming, J., Gaudel, A., Hendrick, F., Huijnen, V., Jones, L., Kapsomenakis, J., Katragkou, E., Keppens, A., Langerock, B., de Mazière, M., Melas, D., Parrington, M., Peuch, V. H., Razinger, M., Richter, A., Schultz, M. G., Suttie, M., Thouret, V., Vrekoussis, M., Wagner, A., and Zerefos, C.: Data assimilation of satellite-retrieved ozone, carbon monoxide and nitrogen dioxide with ECMWF's Composition-IFS, Atmos. Chem. Phys., 15, 5275-5303, doi:10.5194/acp-15-5275-2015, 2015a.

Inness, A., Aben, I., Agusti-Panareda, A., Borsdoff, T., Flemming, J., Landgraf, J. and Ribas, R.: Monitoring and assimilation of early TROPOMI total column carbon monoxide data in the CAMS system, ECMWF Technical Memoranda 838, 10.21957/r528zfho, 2019c.

https://doi.org/10.5194/acp-2022-458
Preprint. Discussion started: 4 July 2022

Inness, A., Ades, M., Agustí-Panareda, A., Barré, J., Benedictow, A., Blechschmidt, A.-M., Dominguez, J. J., Engelen, R., Eskes, H., Flemming, J., Huijnen, V., Jones, L., Kipling, Z., Massart, S., Parrington, M., Peuch, V.-H., Razinger, M., Remy, S., Schulz, M., and Suttie, M.: The CAMS reanalysis of atmospheric composition, Atmos. Chem. Phys., 19, 3515–3556, https://doi.org/10.5194/acp-19-3515-2019, 2019a.

Inness, A., Flemming, J., Heue, K.-P., Lerot, C., Loyola, D., Ribas, R., Valks, P., van Roozendael, M., Xu, J., and Zimmer, W.: Monitoring and assimilation tests with TROPOMI data in the CAMS system: near-real-time total column ozone, Atmos. Chem. Phys., 19, 3939–3962, https://doi.org/10.5194/acp-19-3939-2019, 2019b.

Inness, A.: Model data exp=hmib for research article "Monitoring and assimilation of S5P/TROPOMI carbon monoxide data with the global CAMS near-real time system", ECMWF [data set], https://doi.org/10.21957/ax0c-fm72, 2022a.

Inness, A.: Model data exp=hlxm for research article "Monitoring and assimilation of S5P/TROPOMI carbon monoxide data with the global CAMS near-real time system", ECMWF [data set], https://doi.org/10.21957/ax0c-fm72, 2022b.

John, S. S., Deutscher, N. M., Paton-Walsh, C., Velazco, V. A., Jones, N. B., and Griffith, D. W. T.: "2019–20 Australian Bushfires and Anomalies in Carbon Monoxide Surface and Column Measurements", Atmosphere 12, no. 6: 755, https://doi.org/10.3390/atmos12060755, 2021.

Kaiser, J. W., Heil, A., Andreae, M. O., Benedetti, A., Chubarova, N., Jones, L., Morcrette, J.-J., Razinger, M., Schultz, M. G., Suttie, M., and van der Werf, G. R.: Biomass burning emissions estimated with a global fire assimilation system based on observed fire radiative power, Biogeosciences, 9:527–554, 2012.

Kanakidou, M.; Crutzen, P.J.: "The Photochemical Source of Carbon Monoxide: Importance, Uncertainties and feedbacks", in: Chemosphere, 1: 91–109, 1999.

Krol, M., Houweling, S., Bregman, B., van den Broek, M., Segers, A., van Velthoven, P., Peters, W., Dentener, F., and Bergamaschi, P.: The two-way nested global chemistry-transport zoom model TM5: algorithm and applications, Atmos. Chem. Phys., 5, 417–432, https://doi.org/10.5194/acp-5-417-2005, 2005.

Landgraf, J., aan de Brugh, J., Scheepmaker, R., Borsdorff, T., Hu, H., Houweling, S., Butz, A., Aben, I., and Hasekamp, O.: Carbon monoxide total column retrievals from TROPOMI shortwave infrared measurements, Atmos. Meas. Tech., 9, 4955-4975, https://doi.org/10.5194/amt-9-4955-2016, 2016.

Li, M., Shen, F. & Sun, X.: 2019–2020 Australian bushfire air particulate pollution and impact on the South Pacific Ocean, Sci Rep 11, 12288, https://doi.org/10.1038/s41598-021-91547-y, 2021.

Martínez-Alonso, S., Deeter, M., Worden, H., Borsdorff, T., Aben, I., Commane, R., Daube, B., Francis, G., George, M., Landgraf, J., Mao, D., McKain, K., and Wofsy, S.: 1.5 years of TROPOMI CO measurements: comparisons to MOPITT and ATom, Atmos. Meas. Tech., 13, 4841–4864, https://doi.org/10.5194/amt-13-4841-2020, 2020.

https://doi.org/10.5194/acp-2022-458
Preprint. Discussion started: 4 July 2022

Nedelec, P., Cammas, J.-P., Thouret, V., Athier, G., Cousin, J.-M., Legrand, C., Abonnel, C., Lecoeur, F., Cayez, G., and Marizy, C.: An improved infrared carbon monoxide analyser for routine measurements aboard commercial aircraft: technical validation and first scientific results for the MOZAIC III programme, Atmos. Chem. Phys., 3, 1551-1564, 2003.

Novelli, P.C. and Masarie, K.A.: Atmospheric Carbon Monoxide Dry Air Mole Fractions from the NOAA ESRL Carbon Cycle Cooperative Global Air Sampling Network, 1988-2013, Version: 2014-07-02, ftp://aftp.cmdl.noaa.gov/data/trace_gases/co/flask/surface/ (last access December 2014), 2014.

Ohneiser, K., Ansmann, A., Baars, H., Seifert, P., Barja, B., Jimenez, C., Radenz, M., Teisseire, A., Floutsi, A., Haarig, M., Foth, A., Chudnovsky, A., Engelmann, R., Zamorano, F., Bühl, J., and Wandinger, U.: Smoke of extreme Australian bushfires observed in the stratosphere over Punta Arenas, Chile, in January 2020: optical thickness, lidar ratios, and depolarization ratios at 355 and 532 nm, Atmos. Chem. Phys., 20, 8003–8015, https://doi.org/10.5194/acp-20-8003-2020, 2020.

Oltmans, SJ and Levy II, H: Surface ozone measurements from a global network, Atmos. Environ., 28, 9-24, 1994.

Parrish, D.F. and Derber, J. C.: The National Meteorological Center's spectral statistical-interpolation analysis scheme. Mon. Weather Rev., 120, 1747-1763, 1992.

Pope, R. J., Kerridge, B. J., Siddans, R., Latter, B. G., Chipperfield, M. P., Arnold, S. R., Ventress, L. J., Pimlott, M. A., Graham, A. M., Knappett, D. S., and Rigby, R.: Large enhancements in Southern Hemisphere satellite-observed trace gases due to the 2019/2020 Australian wildfires. Journal of Geophysical Research: Atmospheres, 126, e2021JD034892. https://doi.org/10.1029/2021JD034892, 2021.

Rémy, S., Kipling, Z., Flemming, J., Boucher, O., Nabat, P., Michou, M., Bozzo, A., Ades, M., Huijnen, V., Benedetti, A., Engelen, R., Peuch, V.-H., and Morcrette, J.-J.: Description and evaluation of the tropospheric aerosol scheme in the European Centre for Medium-Range Weather Forecasts (ECMWF) Integrated Forecasting System (IFS-AER, cycle 45R1), Geosci. Model Dev., 12, 4627–4659, https://doi.org/10.5194/gmd-12-4627-2019, 2019.

Seinfeld, J.H. and Pandis, S.N.: Atmospheric Chemistry and Physics: From Air Pollution to Climate Change. 2nd Edition, John Wiley & Sons, New York, 2006.

Sha, M. K., Langerock, B., Blavier, J.-F. L., Blumenstock, T., Borsdorff, T., Buschmann, M., Dehn, A., De Mazière, M., Deutscher, N. M., Feist, D. G., García, O. E., Griffith, D. W. T., Grutter, M., Hannigan, J. W., Hase, F., Heikkinen, P., Hermans, C., Iraci, L. T., Jeseck, P., Jones, N., Kivi, R., Kumps, N., Landgraf, J., Lorente, A., Mahieu, E., Makarova, M. V., Mellqvist, J., Metzger, J.-M., Morino, I., Nagahama, T., Notholt, J., Ohyama, H., Ortega, I., Palm, M., Petri, C., Pollard, D. F., Rettinger, M., Robinson, J., Roche, S., Roehl, C. M., Röhling, A. N., Rousogenous, C., Schneider, M., Shiomi, K., Smale, D., Stremme, W., Strong, K., Sussmann, R., Té, Y., Uchino, O., Velazco, V. A., Vigouroux, C., Vrekoussis, M., Wang, P., Warneke, T., Wizenberg, T., Wunch, D., Yamanouchi, S., Yang, Y., and Zhou, M.: Validation of methane and carbon monoxide from Sentinel-5 Precursor using TCCON and NDACC-IRWG stations, Atmos. Meas. Tech., 14, 6249–6304, https://doi.org/10.5194/amt-14-6249-2021, 2021.

https://doi.org/10.5194/acp-2022-458
Preprint. Discussion started: 4 July 2022

Thomas, J. L., Polashenski, C. M., Soja, A. J., Marelle, L., Casey, K. A., Choi, H. D., Raut, J.-C., Wiedinmyer, C., Emmons, L. K., Fast, J. D., Pelon, J., Law, K. S., Flanner, M. G. and Dibb, J. E.: Quantifying black carbon deposition over the Greenland ice sheet from forest fires in Canada, *Geophys. Res. Lett.*, 44, 7965– 7974, doi:10.1002/2017GL073701, 2017.

van der Velde, I.R., van der Werf, G.R., Houweling, S., Maasakkers, J. D., Borsdorff, T., Landgraf, J., Tol, P., van Kempen, T. A., van Hees, A., Hoogeveen, R., Veefkind, J. P., and Aben, I.: Vast CO_2 release from Australian fires in 2019–2020 constrained by satellite, Nature 597, 366–369, https://doi.org/10.1038/s41586-021-03712-y, 2021.

Veefkind, J. P., Aben, I., McMullan, K., Förster, H., de Vries, J., Otter, G., Claas, J., Eskes, H. J., de Haan, J. F., Kleipool, Q., van Weele, M., Hasekamp, O., Hoogeveen, R., Landgraf, J., Snel, R., Tol, P., Ingmann, P., Voors, R., Kruizinga, B., Vink, R., Visser, H., and Levelt, P. F.: TROPOMI on the ESA Sentinel-5 Precursor : A GMES Mission for global observations of the atmospheric composition for climate, air quality and ozone layer applications, Remote Sensing of Environment, 120:70-83, doi:10.1016/j.rse.2011.09.027, 2012.

Vidot, J., Landgraf, J., Hasekamp, O., Butz, A., Galli, A., Tol, P. and Aben, I. (2021): Carbon monoxide from shortwave infrared reflectance measurements: A new retrieval approach for clear sky and partially cloudy atmospheres. Remote Sensing of Environment, 120:255–266, 2012.

Witze, Alexandra. "The Arctic is burning like never before -- and that's bad news for climate change." Nature, vol. 585, no. 7825, 17 Sept. 2020, pp. 336+. Gale Academic OneFile, link.gale.com/apps/doc/A635608962/AONE?u=urjy&sid=googleScholar&xid=a55139bb. Accessed 5 Apr. 2022.

Worden, H. M., Deeter, M. N., Frankenberg, C., George, M., Nichitiu, F., Worden, J., Aben, I., Bowman, K. W., Clerbaux, C., Coheur, P. F., de Laat, A. T. J., Detweiler, R., Drummond, J. R., Edwards, D. P., Gille, J. C., Hurtmans, D., Luo, M., Martínez-Alonso, S., Massie, S., Pfister, G., and Warner, J. X.: Decadal record of satellite carbon monoxide observations, Atmos. Chem. Phys., 13, 837–850, https://doi.org/10.5194/acp-13-837-2013, 2013.